RO PROCESS OPTIMIZATION BASED ON DETERMINISTIC PROCESS MODEL COUPLED WITH STOCHASTIC COST MODEL

A Thesis
Presented to
The Academic Faculty

By

Pranay P. Mane

In Partial Fulfillment
Of the Requirements for the Degree
Master of Science in Environmental Engineering

Georgia Institute of Technology

May, 2007

RO PROCESS OPTIMIZATION BASED ON DETERMINISTIC PROCESS MODEL COUPLED WITH STOCHASTIC COST MODEL

Dr. Jae-Hong Kim
School of Civil & Environmental Engineering
Georgia Institute of Technology

Dr. Seong-Hee Kim
School of Industrial & Systems Engineering
Georgia Institute of Technology

Dr. Spyros G. Pavlostathis
School of Civil & Environmental Engineering
Georgia Institute of Technology

Date Approved: April 09, 2007

ACKNOWLEDGEMENT

I would like to thank Dr. Jaehong Kim for his giving me this opportunity to learn and for his continuous guidance and support during my entire course of time for my master's study at Georgia Institute of Technology. I would also like to thank Dr. Seong-Hee Kim for her continuous advisement in this study, and Dr. Spyros G. Pavlostathis for serving as my committee member and his suggestions. U.S. Bureau of Reclamation, Carollo Engineers P.C., Saehan Inc. and Hydranautics are acknowledged for providing partial financial support for this project. Finally, I would like to thank Hoon Hyung for his advice and suggestions, Dr. Jong-Sang Park from Saehan Inc. for performing pilot-scale experiments, Dr. Jess Brown from Carollo Engineers P.C. for providing us with valuable data from seawater desalination plants over U.S.

TABLE OF CONTENTS

LIST OF TABLES

LIST OF FIGURES

LIST OF SYMBOLS AND ABBREVIATIONS

Abbreviations

CC – capital costs

CCL2 – Contaminant Candidate List 2

CDHS – California Department of Health Services

CEM – cost estimation model

CP – concentration polarization

MT - mass transfer

OC – operating costs

RO – reverse osmosis

S-CEM – stochastic cost estimation model

TDS – total dissolved solutes

USEPA – U.S. Environmental Protection Agency

WHO – World Health Organization

SUMMARY

A survey performed over existing two pilot-scale and two full-scale RO desalination facilities to study the current status of boron rejection showed a highest rejection 85% leading to permeate boron concentration of 0.52 mg/L, and recent studies predicted a cost increase due to incorporation of boron reduction systems. Mathematical models were developed to study the process performance and related cost implications. The deterministic process model was verified with pilot-scale experiment performed using a single spiral wound module and was later modified to represent the full-scale design options available to meet the required water quality criteria. Then the selected full-scale design options were simulated to predict their performance in terms of recovery and boron rejection.

For cost analysis, to account for uncertainty probability models were developed for stochastic inputs to the cost estimation model and were used with operating parameters from the full-scale simulations to determine the expected total cost of water produced. Later, a sensitivity analysis was performed to observe the effect of change in uncertainty of inputs. Further, the applications of the deterministic process model are suggested.

1. INTRODUCTION

Sea water desalination has been gaining popularity as a feasible option for potable water production, as available water sources are gradually depleting due to water scarcity as well as quality deterioration. High pressure reverse osmosis (RO) processes have been the technology of choice for sea water desalination in the US and many other countries in the world. Recent prosper in membrane processes is attributed to technological developments in the membrane materials and membrane process engineering (Matsuura, 2001; Strathmann, 2001). As a result, average costs of producing potable water from seawater have decreased significantly from $\$2.0/m^3$ to $\$0.5/m^3$ over last decade (Figure 1) (Wilf and Bartels, 2005). While the costs have become more comparable to the other conventional water treatment technologies in recent years, costs are still considered as a limiting factor for widespread application of RO technology for seawater desalination.

Requirement for additional treatment goals, *e.g.*, treatment of emerging contaminants, leads to increase in costs. One of the compounds that have been significantly limiting the RO process application in recent years is boron. Boron exists in sea water at an average concentration of 4.6 mg/L (Nadav 1999; Hyung and Kim, 2006). Since the boron rejection by full-scale RO processes have been typically as low as 43 - 78% presence of excess boron in the product water could be problematic (Magara, Aizawa *et al.,* 1996). For example, a guideline by World Health Organization (WHO) suggests a maximum concentration of 0.5 mg/L of boron in Drinking Water (WHO,

1998). Boron is also listed in the Contaminant Candidate List 2 (CCL2) by U.S. Environmental Protection Agency (USEPA) (EPA, 2005).

The recent study by Hyung and Kim (2006) investigated boron rejection by several seawater RO (SWRO) membranes. A mathematical model was developed to predict boron rejection under different water quality (*i.e.* pH) and operating (*i.e.* pressure and temperature) conditions. Such a model has been proposed as a tool to predict boron rejection with the ultimate goal of optimizing RO-based desalination processes. The primary objective of this study was to expand this lab-scale model into a larger-scale model that can predict boron rejection by full-scale processes employing spiral wound RO elements.

It was also recognized that few studies to date have investigated how the overall process costs are affected by requirement for additional boron removal, especially when stringent boron concentration requirement is enforced by regulating agencies. Such predictions are challenging as cost estimation is based on many uncertain parameters and inherently stochastic. Therefore, another objective of this study was to develop a stochastic-cost estimation model (S-CEM). This model was used to perform comparative analysis on the costs of four representative design options available for boron reduction in SWRO desalination processes.

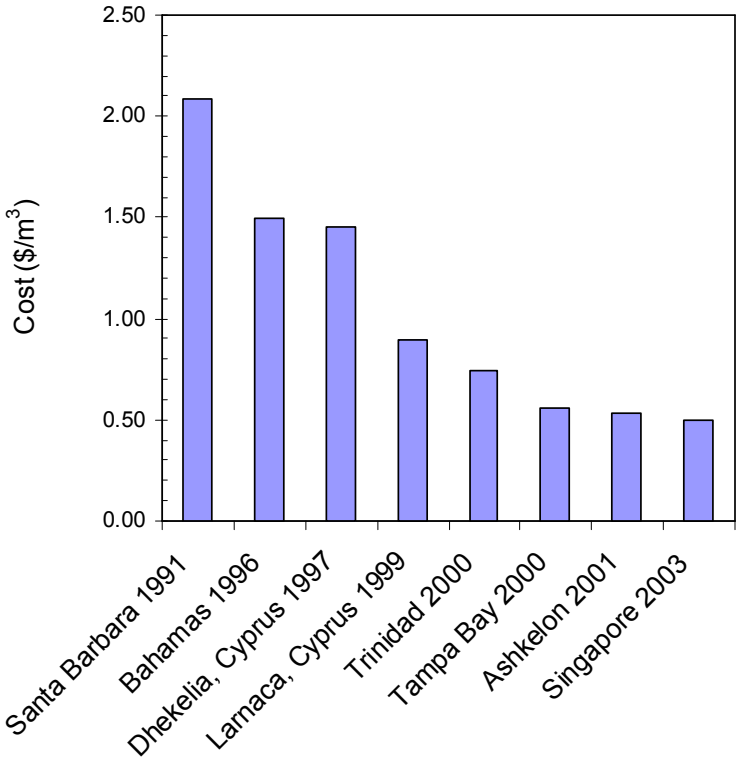

Figure 1. Cost of potable water production from seawater by RO desalination technology at selected seawater desalination plants. (Source: BCC Inc., Market Research, 2005).

2. LITREATURE REVIEW

Although, almost 99 % other ionic species are rejected by seawater RO membranes, boron rejection by RO membranes has been reported to be low consistently (Magara, Aizawa *et al.,* 1996; Nadav, 1999). For example, Magara (1996) reported boron rejection of 43-78 % and permeate boron concentration to a level of 1.3 mg/L in his study over 8 RO desalination plants in Japan, and the a seawater desalination plant in Israel reported a value of 1.8 mg/L, which is far above the regulation (Magara, Aizawa *et al.,* 1996; Nadav, 1999). Though boron is present at a low average concentration of 4.6 mg/L in seawater, but due to low rejection by RO membranes, the boron concentration in permeate water is usually above the suggested guideline by WHO, and in some cases above the current regulation of 1 mg/L set by California Department of Health Services (CDHS) (CDHS, 2006). As boron is being considered one of the major limiting factors in design and operation of full-scale seawater systems, it was desirable to study the performance of existing seawater desalination plants to reject boron from natural seawater through a national reconnaissance study and further predict the plant performance using a full-scale RO process model.

In recent years a significant amount of research has been dedicated to study the effect of operating conditions on boron transport through RO membrane (Sagiv and Semiat 2004; Taniguchi, Fusaoka *et al.,* 2004). From these research, temperature and pH have been identified as the factors that significantly affect the passage of boron through the membrane (Sagiv and Semiat, 2004). Pressure *per se* does not affect the boron transport, however higher operating pressures lead to high recovery and effectively

diluting the boron in permeate and leading to higher overall boron rejection. Considering above factors, a permeability equation has been in need that accounts for the effect of pH and temperature on boron permeability.

Boron is present in form of boric acid (H_3BO_3) and borate ions ($H_2BO_3^-$) in water depending upon the pH of seawater and the first acid dissociation constant (pKa_1) of boric acid. Boric acid has a pKa_1 of 9.14 in natural water; however, the value is less than for seawater because of high salinity and has a value equal to 8.68 in seawater at a representative salt (TDS) concentration of 34,000 mg/L and a temperature of 25^{o}C (Hyung and Kim, 2006). Therefore, the pH of feed solution is the most important parameter that primarily influences the speciation of boric acid in water and consequently the boron passage through the RO membrane in seawater desalination process (Nadav 1999; Taniguchi, Kurihara *et al.,* 2001; Redondo, Busch *et al*., 2003; Taniguchi, Fusaoka *et al.,* 2004; Wilf and Bartels, 2005). Earlier efforts to quantify boron concentration in permeate water (C_{pb}) by relating it to salt (TDS) concentration in permeate water (C_p), and relating boron permeability (P_{sb}) to salt (TDS) permeability (P_s), have reasonably quantified boron concentration in product water (Taniguchi, Kurihara *et al.* 2001; Sagiv and Semiat, 2004). However, considering the influence of pH on speciation of boron in seawater and selective rejection of species by RO membrane, a model based on a mechanistic approach for boron transport has been in need to predict the performance of process to reject boron in seawater desalination process at different pH and temperature. The recently developed model for boron permeability which relates the solute permeability parameter (B_{sb}) and reflection coefficient (σ_{sb}) to pH and temperature (^{o}C) of

the solution, to account for speciation of boric acid in water, is used in this study to quantify boron concentration in permeate water (Hyung and Kim, 2006).

Cost is the critical parameter that aids decision making in almost all fields and is the most important parameter controlling the selection of a RO process from different available alternatives. Since cost of a RO process is a dependent variable of several other independent variables as unit cost of membranes, energy, chemicals etc., and process operating parameters e.g. pressure, flow rate, recovery, feed salt concentration etc; determining the actual cost of the process is difficult (Parekh 1988; Cardrew, 1998). As a result, selection of the best design option is often based on cost comparisons of available configurations performing under standard (ideal) operating conditions, by using a cost-estimation model (CEM). Several CEM's based on empirical relations have been suggested in literature to compare the scenarios and select the system having lowest unit cost of producing water along with desired water quality performance (Malek, Hawlader *et al.,* 1996; Maskan, Wiley *et al.,* 2000; Helal, El-Nashar *et al.,* 2003). The independent variables such as membrane costs, energy costs, interest rates, discount rates, feed pressure, flow rate etc. are used as inputs to these CEM's determine the total unit cost of water produced and considering profitability in future. However, the variables used in cost analysis *e.g.* membrane costs, energy costs; interest rates etc., are random in nature, therefore making the total cost of water uncertain in nature. As a result, a meaningful conclusion can only be made using a CEM, if the risk involved in the total cost and future profitability are assessed by considering the uncertainty in inputs. This risk (uncertainty) in the total cost and future profitability can be assessed by using a stochastic cost-estimation model (S-CEM).

In a deterministic CEM, the inputs, have fixed value, and the CEM yields a definite, or deterministic, solution. Stochastic models, on the other hand, include the effect of uncertainty in the inputs and lead to a solution that can be quantified by its expected value and probability. Inputs recognized to entail uncertainty to the output are assumed to be random and independently and identically distributed (I.I.D.) in nature. Uncertainty may also exist in process models parameters due inadequate representation of the physical process, lack of information about process parameters and the determination method of empirical coefficient. However, the RO process is deterministic as compared to the conventional water/wastewater treatment process, where the particle size, influent concentration of contaminants and pathogens, oxygen content etc. are uncertain and therefore random in nature. In that case it is necessary to assess the uncertainty in the outputs of the process model so that there is a high probability of meeting the standards for drinking water or the effluent sewage. However in case of a RO process, the feed concentration of solutes, the feed flow rate, feed pressure are quite deterministic, and therefore, a deterministic process model can be used for a RO process.

3. MODEL DEVELOPMENT

Computer modeling provides a useful tool to predict the performance of SWRO processes with different design options under different operating conditions. Basic transport equations and mathematical models for spiral wound module and system of spiral wound modules are discussed in detail below.

3.1. Governing Equations for Deterministic Process Model

3.1.1. Spiral Wound Element Model

The membrane leaf (consisting of filtration channel i.e. a feed flow channel and a permeate flow channel) is divided in m = 10 and n = 10 segments (oriented in orthogonal directions), each of distance Δx and Δy respectively to form a grid, as shown in Figure 2. The dimensions of the finite element *i.e.* Δx and Δy are obtained as:

$$\Delta x = L / m \quad (1)$$

$$\Delta y = W / n \quad (2)$$

, where L = length of the membrane leaf (along the spiral wound module) [m; L]; W = width of membrane leaf (orthogonal longitudinal axis of spiral wound module) [m; L]. The input parameters to model Q_{f0}, P_{f0} and C_{f0}, are the operating parameters for the first element of the grid.

3.1.2. Water and Solute Transport

A phenomenological Spiegler and Kedem model was used to predict water and solute transport as follows (Spiegler and Kedem, 1966):

$$J_v(i,j) = A \cdot \left\{ \left[(P_f(i,j) - P_p(i,j) \right] - \sigma \cdot \left[\pi_w(i,j) - \pi_p(i,j) \right] \right\} \quad (3)$$

$$J_s(i,j) = B\left[C_w(i,j) - C_p(i,j) \right] + \left(1-\sigma\right) J_v(i,j) \cdot \overline{C} \quad (4)$$

, where J_v = volumetric water flux [$m^3/m^2 \cdot s$; LT^{-1}]; J_s = gravimetric solute flux [$mol/m^2 \cdot s$; $ML^{-2}T^{-1}$]; A = hydraulic transport parameter [$m/(Pa \cdot s)$; $M^{-1}L^2T$]; B = solute transport parameter [m/s; LT^{-1}]; σ = reflection coefficient which indicates the degree of water/solute coupling [dimensionless]; P = hydraulic pressure [Pa; $ML^{-1}T^{-2}$]; π = osmotic pressure [Pa; $ML^{-1}T^{-2}$]; C = superficial aqueous-phase solute concentration which is assumed to be in equilibrium with concentration of solute in the membrane phase [mol/m^3; ML^{-3}]; $\overline{C}$ = arithmetic average of concentration of solute across the membrane phase [mol/m^3; ML^{-3}]; i = index number along x axis; j = index number along y axis.

3.1.3. Concentration Polarization

Concentration polarization is one of the most important factors limiting performance of nearly all membrane separation processes (Strathmann, 1981). CP effect

leads to increased flow resistance and the solute passage through the membrane, thereby reducing permeate flux and rejection of solutes. Therefore, designing of a reverse osmosis system requires a fair prediction of CP phenomenon. The steady state concentration of solute at the membrane wall (i.e. in the CP layer) can be determined by following nonlinear relationship (Marinas and Urama, 1996).

$$[C_w(i,j) - C_p(i,j)] = [C_f(i,j) - C_p(i,j)] \cdot \exp\left(\frac{J_v(i,j)}{k(i,j)}\right) \quad (5)$$

, where C_w = concentration of solute adjacent to membrane wall [mol/m^3; ML^{-3}]; C_p = concentration of solute in permeate [mol/m^3; ML^{-3}]; C_f = concentration of solute in the feed solution [mol/m^3; ML^{-3}]; J_v = volumetric flux of water through membrane [m^3/(m^2·s); LT^{-1}]; and k = mass transfer coefficient [m/s; LT^{-1}]. In this study, CP layer is assumed to be fully developed, and a simple non-linear mathematical equation with a lumped parameter approach is used to predict the degree of concentration polarization, as compared to various numerical models based on distributed parameter approaches (Bhattacharya and Hwang, 1997; Kim and Hoek, 2005).

3.1.4. Mass Transfer Coefficient

Several mass transfer coefficient relationships have been developed in the past, as briefly reviewed by Gekas and Hallstrom (1987). The mass transfer through RO membrane is influenced by geometry of spacers (turbulence promoters), geometry of feed

flow channel (thickness), fluid properties (dynamic viscosity and velocity) and the solute properties (diffusivity). The presence of the turbulence promoters in spiral wound module needs to be accounted for, because it leads to increased mass transfer as the laminar boundary layer thickness reduces due to turbulence. Considering above factors, an empirical equation that includes the effect of all of the above parameters would best serve the purpose of developing a design and simulation model. Therefore, a generic empirical equation developed by Winograd *et al.* (1973) to predict the mass transfer in narrow channels in presence of turbulence promoters is used in this study, based on a sensitivity analysis presented in later part of this study (Winograd, Solan *et al.,* 1973):

$$k = 0.753\left(\frac{2K}{2-K}\right)^{0.5}\left(\frac{D}{h_b}\right)S_c^{(-1/6)}\left(\frac{P_e \cdot h_b}{\Delta L}\right)^{0.5} \tag{6}$$

, where, k = mass transfer coefficient [m/s; LT^{-1}]; K = 0.5 = efficiency of mixing net [dimensionless]; D = diffusion coefficient [m^2/s; L^2T^{-1}]; h_b = thickness of the feed channel [m; L]; h_p = thickness of permeate channel [m; L]; S_c = Schmidt number = $\mu/\rho D$, [dimensionless]; P_e = Peclet number = $2h_bU_b/D$, [dimensionless]; ΔL = 0.006 m = characteristic length of mixing net [m; L].

3.1.5. Osmotic Pressure

Following empirical equations developed by Miyake (1939) and Sekino (1991) are used to estimate osmotic pressure, density, dynamic viscosity and diffusivity of water with high salt content (Taniguchi and Kimura, 2000):

Osmotic pressure (Miyake, 1939):

$$\pi(C,T)=(0.6955+0.0025T)\times 10^{8}\cdot\left(\frac{C}{\rho}\right) \tag{7}$$

Density (Sekino, 1991):

$$\rho=498.4M+\sqrt{248,400M^{2}+752.4MC}\text{ , (Where }M=1.0069-2.757\times 10^{-4}T\text{)} \tag{8}$$

Diffusion coefficient (Sekino, 1991):

$$D=6.725\times 10^{-6}\cdot\exp\left(0.1546\times 10^{-3}C-\frac{2,513}{273.15+T}\right) \tag{9}$$

And, Dynamic Viscosity (Sekino, 1991):

$$\mu=1.234\times 10^{-6}\cdot\exp\left(0.00212C+\frac{1,965}{273.15+T}\right) \tag{10}$$

, where, π = Osmotic pressure [Pa; $ML^{-1}T^{-1}$]; C = concentration of salts (TDS) [kg/m^3; ML^{-3}]; T = temperature [^{o}C; T]; ρ = density [kg/m^3; ML^{-3}]; D = diffusion coefficient of salt [m^2/s; L^2T^{-1}]; μ = dynamic viscosity [Pa·s; $ML^{-1}T^{-1}$].

3.1.6. Pressure Drop

The flow pattern in feed channel and permeate channel are oriented in orthogonal directions (as described in section 3.1.1). The pressure drop in these two channels over

an infinitesimal element 'Δx' & 'Δy' can be calculated by the following equations (Senthilmurugan, Ahluwalia *et al.,* 2005):

$$P_f(i\text{-}1,j) - P_f(i,j) = H_b \; n_F U_f^{(n_F-1)} \sum_{1}^{i\text{-}1} \left(\frac{2J_v(i,j)}{h_b} \right) \tag{11}$$

$$P_p(i,j+1) - P_p(i,j) = H_p \sum_{j+1}^{n} \left(\frac{2J_v(i,j)}{h_p} \right) \tag{12}$$

Where,

$$H_b = k_{fb} \mu \Delta x^2 \tag{13}$$

$$H_p = k_{fp} \mu \Delta y^2 \tag{14}$$

, where P_f = pressure in feed channel (feed side) [Pa; $ML^{-1}T^{-2}$]; P_p = pressure in permeate channel (permeate side) [Pa; $ML^{-1}T^{-2}$]; Δx = element along x axis [m; L]; Δy = element along y axis [m; L]; μ = dynamic viscosity [Pa·s; $ML^{-1}T^{-1}$]; J_v = permeate flux [$m^3/(m^2 \cdot s)$; LT^{-1}]; h_b = depth of feed channel [m; L]; h_p = thickness of permeate channel [m; L]; n_F = dimensionless constant parameter[dimensionless]; k_{fb} = friction parameter for feed channel [$(1/m^2)$; L^{-2}]; k_{fp} = friction parameter for permeate channel [$(1/m^2)$; L^{-2}].

The applicable boundary conditions for the above equations are as follows:

$$P_f = P_{f0}, \text{ at } x = 0 \quad (15)$$

$$P_p = P_{atm}, \text{ at } y = 0 \quad (16)$$

, where P_{atm} = atmospheric pressure (assumed to be equal to pressure in permeate at outlet) = 1.013×10^5 Pascal. Above pressure drop equations are derived based on the assumption that the Darcy's law is applicable for flow through narrow channels and the dimensionless constant $n_F = 1$.

3.1.7. Boron Transport

The following Equations (17) and (18) developed by Hyung and Kim (2006) are used to predict permeability coefficient and reflection coefficient of boron at different pHs and temperatures:

$$B_{s(B)} = \alpha_0 \times B_{s(H_3BO_3)25} \exp\left(a\left(t-298\right)\right) + \alpha_1 \times B_{s\left(H_2BO_3^-\right)\ 25} \exp\left(b\left(t-298\right)\right) \quad (17)$$

$$\sigma_B = \alpha_0 \times \sigma_{(H_3BO_3)} + \alpha_1 \times \sigma_{(H_2BO_3^-)} \quad (18)$$

, where $B_{s(B)}$ = overall permeability constant of boron [m/s; LT^{-1}]; $B_{s(H3BO3)25}$ = permeability constant of boric acid (H_3BO_3) estimated at 25°C [m/s; LT^{-1}]; $B_{s(H2BO3-)25}$ = permeability constant of borate ($H_2BO_3^-$) estimated at 25°C [m^2/s; L^2T^{-1}]; α_0 *and* a_1 =

fraction of boric acid and borate, respectively (Dimensionless); and t = absolute temperature [K; θ]; $\sigma_{(H3BO3)}$ = reflection coefficient of boric acid [dimensionless] and $\sigma_{(H2BO3-)}$ = reflection coefficient of borate ion [dimensionless]. In the above equations, α_0 and α_1 represent the fraction of boric acid and borate ion, respectively. Values of empirical constants, a and b need to be determined experimentally for different membranes.

3.1.8. Material Balance and Performance

The equations (1) to (18) are solved for this RO membrane grid element by using the algorithm as shown in figure. 'fsolve' function in MATLAB® was used to solve the set of nonlinear differential equations, to determine $Q_{p,}$ C_p, and C_w. The input parameters for the next grid element are determined by performing a material balance on the solute and water as given below-

$$Q_p(i,j) = 2 \cdot J_v(i,j) \cdot \Delta x \cdot \Delta y \tag{19}$$

$$Q_f(i+1,j) = Q_f(i,j) - Q_p(i,j) \tag{20}$$

$$C_f(i+1,j) = \frac{Q_f(i,j) \cdot C_f(i,j) - Q_p(i,j) \cdot C_p(i,j)}{Q_f(i+1,j)} \tag{21}$$

And the pressure drop is measured using equations (11) and (12). Further, the

boron transport can be predicted using equations (3), (4), (5), (17) and (18). The overall permeate balance and solute balance is used to calculate the overall recovery and overall rejection in a spiral wound module element, respectively.

$$Q_{pT} = n_L \cdot \sum_{i=1}^{m} \sum_{j=1}^{n} Q_p(i,j) \tag{22}$$

$$\text{Overall permeate recovery} = \frac{Q_{pT}}{Q_{f0}} \tag{23}$$

Similarly,

$$C_{pT} = \frac{n_L \cdot \sum_{i=1}^{m} \sum_{j=1}^{n} Q_p(i,j) \cdot C_p(i,j)}{Q_{pT}} \tag{24}$$

$$\text{Overall rejection} = \left(1 - \frac{C_{pT}}{C_{f0}}\right) \tag{25}$$

, where Q_f = feed flow rate [m^3/day; L^3T^{-1}]; Q_p = permeate flow rate [m^3/day; L^3T^{-1}]; J_v = water flux through RO membrane [$m^3/(m^2 \cdot s)$; LT^{-1}]; C_f = salt (TDS) concentration in feed channel [Kg/m^3; ML^{-3}]; C_p = salt (TDS) concentration in the permeate channel [Kg/m^3; ML^{-3}]; Q_{pT} = total permeate flow rate [m^3/day; L^3T^{-1}]; C_{pT} = Overall salt (TDS) concentration in the product water [Kg/m^3; ML^{-3}]; n_L = number of membrane leaves

[dimensionless]; i = index number along 'x' axis [Dimensionless]; j = index number along 'y' axis [dimensionless].

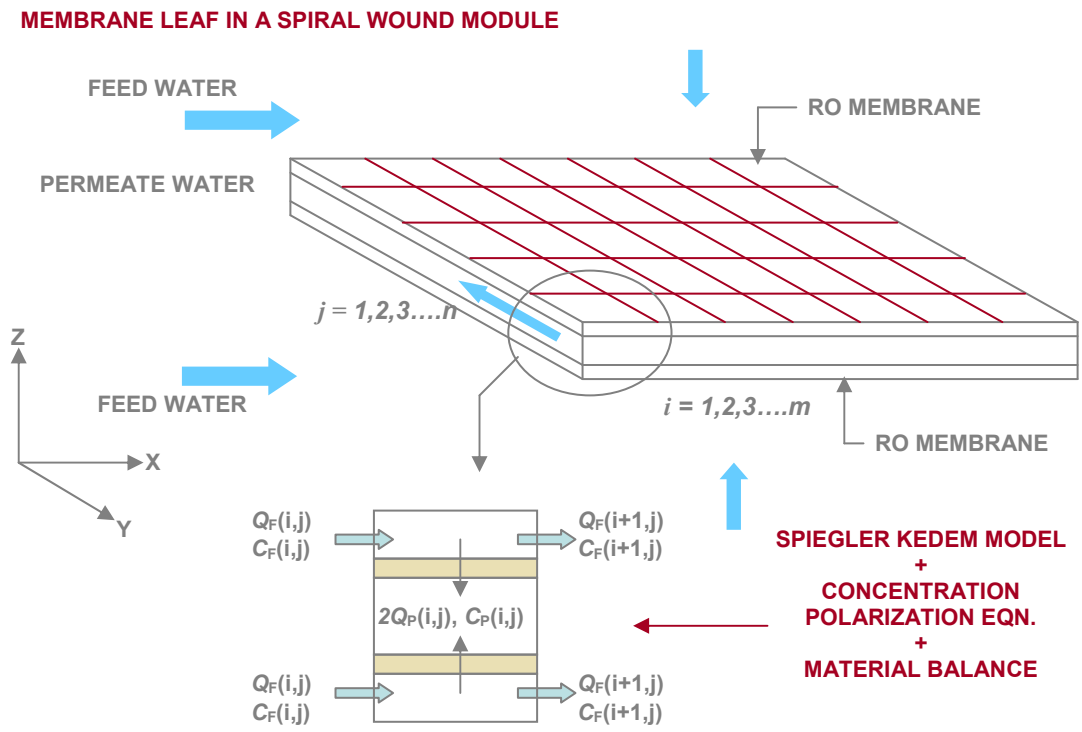

Figure 2. . Membrane leaf divided into grid elements along X and Y axis. The flow in the feed channel is along X axis while in permeate channel is along Y axis, as shown. The elements are represented by index numbers i and j along X and Y respectively.

3.1.9. Full-scale RO Unit Design

Full-scale RO process model consists of an array of pressure vessels, each holding 2 to 8 spiral wound elements in series, as shown in Figure 3. Therefore, material balance and performance relationships given in Equations (19) to (25) for each spiral wound module are solved in series to predict the performance of each pressure vessel. Then the

solutions from each pressure vessels are linearly combined to predict the performance of whole full-scale systems.

The feed pressure at the end of the membrane leaf is different in all grid elements. The values for the above parameters are averaged to determine the input parameters to the following spiral wound element model. The other factors affecting the flow rate and pressure losses are assumed to negligible.

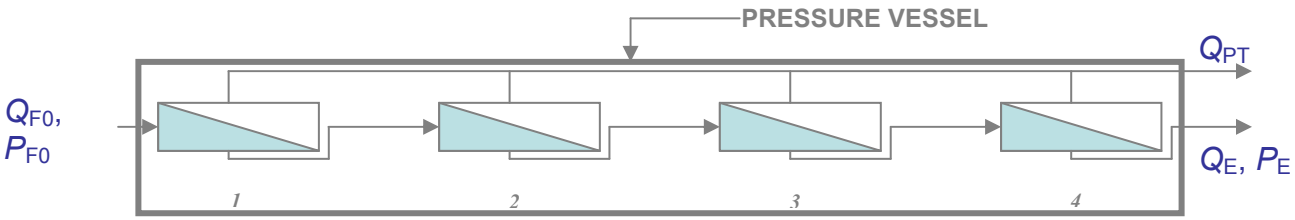

Figure 3. Spiral wound elements in series, in a pressure vessel to represent the full-scale RO process. Simple material balance relationships are used to develop a full-scale simulation model from a spiral wound element model.

3.2. Cost Estimation

3.2.1. Costs of RO Process

Unit costs of producing potable water by seawater RO desalination are primarily comprised of capital costs and the operating costs for the plant. Therefore, costs of a RO process are broadly classified as capital costs (CC) and operating costs (OC). The capital costs (CC) are further divided as direct costs and indirect costs (Parekh, 1988). Direct costs are comprised of mainly (1) seawater intake and pretreatment equipment costs (CC_{IP}), (2) high pressure pump costs (CC_{HP}), (3) RO equipment costs (CC_{RO}), (4)

pressure exchanger cost (CC_{PX}), and (5) ion-exchanger cost (CC_{IX}), which constitute the major share of capital costs. The seawater intake costs and pretreatment equipment costs (CC_{IP}) include the costs for its construction as well; RO equipment costs include the membrane elements costs (CC_{ME}), pressure vessel costs (CC_{PV}), and the RO train costs (CC_{TR}). The total capital costs (CC) are therefore obtained by adding all of the above costs. Since the indirect costs are not directly related to the objective of this study, they are excluded.

The total operating costs (OC) consist of (1) electricity (energy) cost (OC_{EN}), (2) chemical costs (OC_{CH}), (3) membrane replacement costs (OC_{ME}), (4) maintenance costs (OC_{MN}), and (5) labor costs (OC_{LB}). The operating costs of the RO process are relatively high as compared to other water treatment process due to high energy consumption. On the other hand, their capital costs are comparable to the other water treatment alternatives. Therefore, energy consumption plays an important role in controlling the costs of RO process. The energy costs comprise approximately 20 to 30 % of the total costs and approximately 50 % of the operation costs, in a RO process of seawater desalination (Cardona, Culotta, *et al.,* 2003). The energy cost is approximately a linear function of the overall product recovery (R) of the process. Therefore, recovery of the RO process is considered as the most important factor controlling the economics of desalination (Wilf and Klinko, 2001).

3.2.2. Cost Estimation Model

Empirical relationships to determine the costs of components are obtained from previously developed CEM's (Malek, Hawlader *et al.*, 1996; Helal, El-Nashar *et al.*,

2003). In process economics, most of the relations to determine the capital cost or the operating costs are usually based on personal experience of experts or developed from case studies on that particular process (Parekh, 1988; Malek, Hawlader *et al.,* 1996; Helal, El-Nashar *et al.,* 2003). As a result, the unit cost of water determined by CEM's is representative and large differences may results from the estimator's bias (Cardrew, 1998). Different CEM are available depending upon the level of estimate required. For performing feasibility study or comparing scenarios, a "study estimate" is generally used. A study estimate has an accuracy of 30 percent and can be prepared with minimum data at a low cost (Cardrew, 1998).

a. Seawater Intake and Pretreatment Facility

Seawater intake and pretreatment systems (equipment and construction) costs can be estimated as (Malek, Hawlader *et al.* 1996):

$$CC_{PI} = 1.423 \times 996 \cdot (Q_f)^{0.8} = 1417.3 \cdot (Q_f)^{0.8} \quad (26)$$

, where, CC_{IP} = cost of pretreatment and seawater intake system [$]; Q_f = Feed flow rate [L^3T^{-1}; m^3/day]. Marshall and Swift Index = 1.42, to represent the cost in 2005.

The operating costs of seawater intake and pretreatment system consist of the costs of power for operating intake pumps and the costs of chemicals used in pretreatment. As the costs of operating pretreatment system are mostly chemical, the electricity costs associated with the chemical dosing system are assumed to be negligible.

From the experts opinion, the chemical cost are 0.0225 \$/m^3 of feed water (Hyung 2006). Therefore, the total operating costs of the seawater intake and pretreatment system are (Malek, Hawlader *et al.,* 1996):

$$OC_{IP} = \frac{P_O \cdot Q_f \cdot D}{\eta_{IP}} \times PLF + 0.0225 \cdot (Q_f) \tag{27}$$

, where, P_0 = outlet pressure generated by seawater intake pumps [psi]; Q_f = feed flow rate [m^3/day]; PLF = plant load factor = 0.9 [dimensionless]; D = unit cost of electricity [cents/kW-hr]; η_{IP} = efficiency of seawater intake pump = 0.74 [dimensionless].

b. High Pressure Pumps

High pressure pumps comprise a large portion of the capital costs and are difficult to quantify as the costs of pump are not a linearly related with the feed flow capacity. The capital costs can be described as follows (Malek, Hawlader *et al.* 1996) -

$$CC_{HP} = \begin{cases} (562776 + 15337 \cdot P_f) & , for\, Q_f > 10{,}800\ (m^3/d) \\ 116 \cdot (P_f \cdot Q_f)^{0.96} & , for\, 4{,}800\ m^3/d < Q_f \le 10{,}800\ m^3/d \\ 75 \cdot (P_f \cdot Q_f)^{0.96} & , for\, Q_f \le 4{,}800\ m^3/d \end{cases}$$

The operating costs of high pressure pumps are calculated from the power consumption in the pumping process (Malek, Hawlader *et al.,* 1996; Hyung, 2006):

$$OC_{HP} = \frac{0.027 \cdot Q_f \cdot P_f}{\eta_{mo} \cdot \eta_{pm}} \times D \tag{29}$$

, where, Q_f = feed flow rate (m^3/hr); Pf = feed pressure (Psi); D = electricity price (cents/KW-hr);

c. RO Equipment Costs

The RO equipments cost can be divided as membrane element costs (CC_{ME}), pressure vessel costs (CC_{PV}), and trains costs (CC_{TR}) as follows (membrane costs are assumed to be same for seawater reverse osmosis (SWRO) and brackish water reverse osmosis (BWRO) membranes):

$$CC_{ME} = C_{ME} \cdot N_{ME} \tag{30}$$

, where, CC_{ME} = capital cost of membrane elements [$]; C_{ME} = unit cost of membrane element = 500 [$/each]; N_{ME} = total number of membrane elements used in the design [dimensionless].

The pressure vessel costs and the train costs are function of the number of pressure vessels used. The unit cost of pressure vessel is 2,400 $/each and 1,700 $/each, for SWRO and BWRO pressure vessels respectively. Similarly the cost of trains is 4,440 $/PV and 2,910 $/PV.

$$CC_{PV} = C_{PV} \cdot N_{PV} \tag{31}$$

$$CC_{TR} = C_{TR} \cdot N_{PV} \tag{32}$$

, where, CC_{PV} = capital cost of pressure vessels [$]; C_{PV} = unit cost of pressure vessel [$/each]; N_{PV} = number of pressure vessels [dimensionless]; CC_{TR} = capital cost of RO trains [$]; C_{TR} = unit cost of RO train [$/pressure vessel].

Therefore the total capital cost of RO equipments is obtained by adding the above costs:

$$CC_{RO} = CC_{ME} + CC_{PV} + CC_{TR} \tag{33}$$

, where, CC_{RO} = capital cost of RO equipments [$].

d. Pressure Exchanger Costs

Pressure exchangers are used for converting the pressure in concentrate to electricity and further reduce the energy costs. The cost of pressure exchanger is assumed to be a function of the concentrate flow rate of the concentrate and is given as follows (Lu, Hu *et al.*, 2006) -

$$CC_{PX} = 3134.7 \cdot Q_C^{0.58} \tag{34}$$

, where, CC_{PX} = capital cost of pressure exchanger [$]; Q_C = concentrate flow rate [m^3/day].

The cost of energy recovered by the pressure exchanger is given as (Malek, Hawlader *et al.,* 1996) -

$$OC_{PX} = 0.027 \cdot Q_C \cdot P_c \cdot \eta_{PX} \cdot D \tag{35}$$

, where, OC_{PX} = cost of energy recovered from pressure exchanger [$]; Q_C = concentrate flow rate [m^3/hr]; P_C = pressure head in concentrate [bar]; η_{PX} = efficiency of pressure exchanger [dimensionless].

e. Ion-Exchange Equipment Costs

Boron specific ion-exchangers are coupled with a SWRO membrane array to reduce the boron concentration in permeate. These systems are generally termed as hybrid systems, where a less than 50 % of permeate obtained from SWRO membrane array is passed through this ion-exchanger. The cost of 70 m^3/hr capacity ion-exchanger is approximately $150,000.00 (Hyung *et al.* 2006).

4. MATERIALS AND METHODS

4.1. Pilot scale experiments

4.1.1. Experimental setup and membrane module characteristics

Pilot scale experiments were performed using a custom made pilot scale membrane tester (Saehan Industries Inc., Kyungsan, Korea) which holds a spiral wound membrane module with 10.16 cm (4 inch) nominal diameter and 101.6 cm (40 inch) effective length . The experiment was performed using two commercially available pilot-scale RO membranes RE4040-SR and RE4040-SH, manufactured by Saehan Industries Inc. (Kyungsan, Korea). RE4040-SR and RE4040-SH are Thin Film Composite (TFC) type high rejection Polyamide (PA) RO membrane element for seawater desalination. Table presented in Appendix A describes the relevant characteristics and performance parameters for the spiral wound membrane module used for pilot scale experiments and full scale simulations.

4.1.2. Experimental and analytical procedures

The membrane module was first operated with DI water at feed pressure 800 psi for time period of 24 hours. After the flux was stabilized, synthetic seawater containing 10,500 mg/L sodium, 19,000 mg/L chloride, 1,350 mg/L magnesium, 450 mg/L calcium,

2,700 mg/L sulfate and 5 mg/L boron (total dissolved solids of 33,000 mg/L) was applied to the system. The feed pH was changed from 6.2 to 9.5 (6.2, 7.5, 8.5, and 9.5) and feed pressure was changed from 600 to 800 psi (600, 650, 700, 750, and 800), to form an orthogonal matrix of experimental operating conditions. The overall permeate recovery was maintained constant at 8 % (i.e. $Q_{pT}/ Q_{f0} = 0.08$) and temperature T at 25^{o}C. After collecting a feed and permeate from each condition, conductivities of samples were measured by Hach Ion5 conductivity meter (Loveland, CO). Concentrations of boron was measured using an Inductively Coupled Plasma Mass Spectrometer-Atomic Emission Spectroscopy (ICP-AES) (Model ICAP 61E Trace Analyzer, Thermo Jarrell Ash, Franklin, MA) equipped with an autosampler. Feed water pH was monitored using a Thermo Orion 230+ pH meter (Waltham, MA).

4.2. Parameters

Solute Transport Parameter (B) and Hydraulic Transport Parameter (A)

The hydraulic transport parameter (A) and the solute (TDS) transport parameter (B) need to be determined for the membrane used in the pilot-scale element. An iterative algorithm (Appendix D) is used to determine A and B values from pilot-scale experimental data. Initially the assumed A and B values (close to the actual) along with the operating conditions (i.e. feed pressure (P_f), feed flow rate (Q_f) and feed TDS concentration (C_f)) are used as inputs to the deterministic process model developed in the previous part, to predict the values of permeate flow rate (Q_p) and permeate TDS

concentration (C_p). The predicted values for above parameters are compared with the experimental results to determine converge1 and converge2 values as follows:

$$\text{converge1} = \frac{(Q_P)_{predicted}}{(Q_P)_{observed}} \tag{36}$$

$$\text{converge2} = \frac{(C_P)_{predicted}}{(C_P)_{observed}} \tag{37}$$

The converge1 and converge2 values approach unity as A and B reaches the accurate values. Therefore, the convergence criteria are based on the deviation of converge1 and converge2 values from unity:

$$E1 = |1 - \text{converge1}|, \text{ and } E1 \leq 0.001 \tag{38}$$

$$E2 = |1 - \text{converge2}|, \text{ and } E2 \leq 0.001 \tag{39}$$

If the assumed values of A and B satisfy the convergence criteria, they are considered acceptable. Otherwise the assumed values are changed as follows:

$$A = \frac{A}{\text{converge1}} \tag{40}$$

$$B = \frac{B}{converge2} \tag{38}$$

Same procedure is repeated using the new A and B values until the convergence criteria stated in equation (38) and (39) are satisfied.

4.3. Input Models

The unit costs or the rates used as inputs to the CEM are stochastic in nature *i.e.* they are random in nature for which average properties can be predicted. To account for the uncertainty in their occurrence, input probability models are developed based on the data available from previous years. The data was assumed to be random in nature, and independent & identically distributed (I.I.D.). The different available probability distributions are fit to the available data using @Risk, which is commercially available financial simulation software. And the best distribution is selected based on "chi-square" test value, "p-value", and "q-q" (fitted quantile vs. input quantile) plots.

The distributions are developed based on the assumption that the data are random. However, in true case, the data may represent a time-series pattern, which can be evaluated by determining the lag-1 correlation values for the previous data. The values close to 1 represent a time-series pattern. The lag-1 correlation values can be calculated for a given data set by following relation:

$$Lag-1=\frac{\sum_{i=1}^{N-1}(X_i-\overline{X})(X_{i+1}-\overline{X})}{\sum_{i=1}^{N}(X_i-\overline{X})^2} \quad (39)$$

, where $\overline{X}$ = sample mean; i = index number.

The accuracy of the predictions by the stochastic simulations depends upon the ability of the input model to fairly represent the uncertainty in the parameters. There are no "true" models to represent any stochastic input. Therefore, a best approximation is made to obtain useful results. Since the main objective of this study was to develop an approach more importance was given to developing algorithm than developing state-of art input probability models. In many cases, it is difficult to acquire or use data from previous years due to unavailability or discrepancy in available data. In such cases, uniform distributions with predicted minimum and maximum values were assumed for the inputs with no previous data available. Figure 4 shows the trend for electricity prices, discount rates, inflation rates and interest rates -

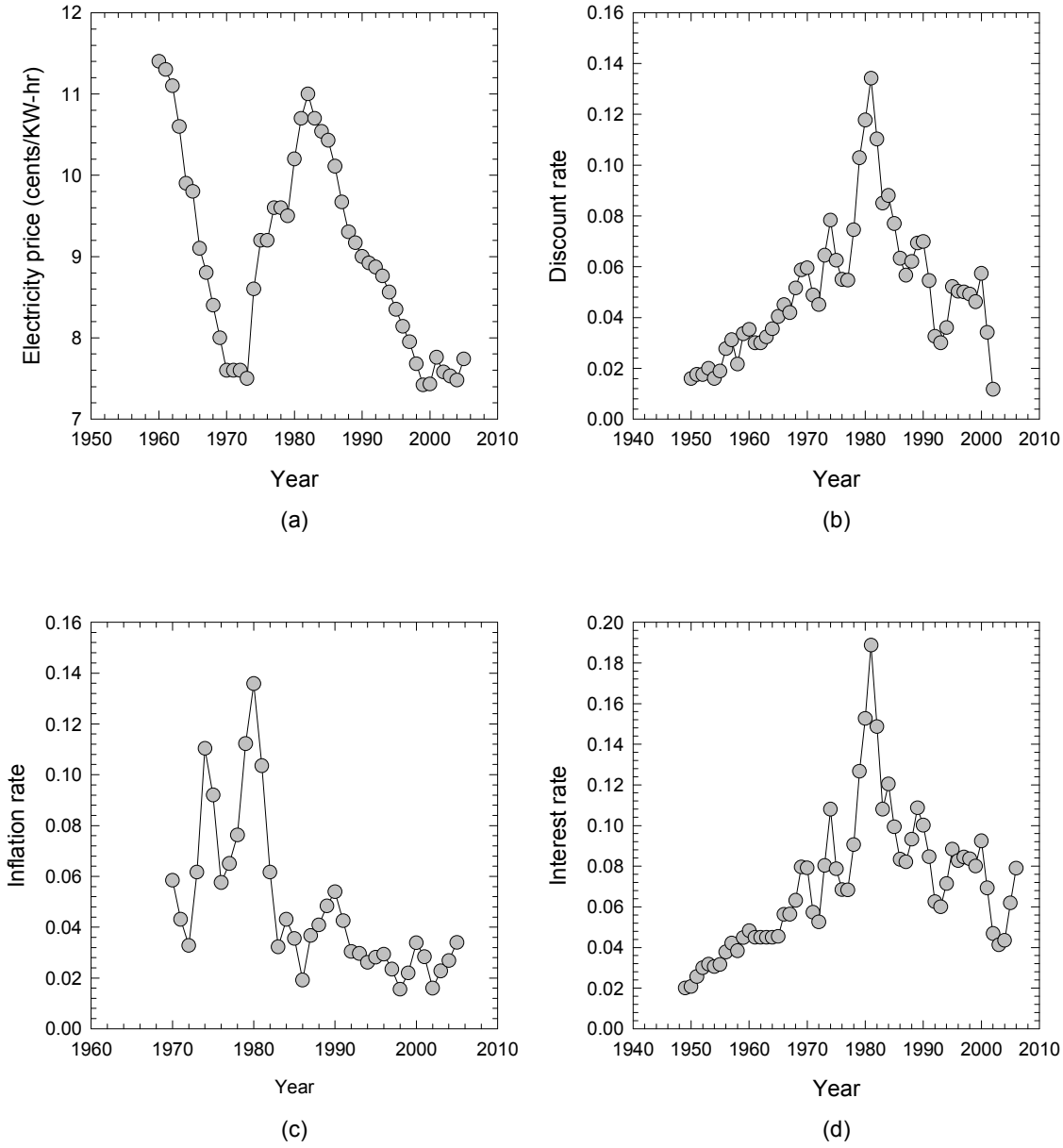

Figure 4. Previous years data for (a) electricity pricing (source aannual energy review, 2005) (b) discount rate (source: ECONOMIC RESEARCH, ST. LOUIS FEDERAL RESERVE BANK) (c) inflation rate (source: inflation data dot com) (d) interest rate (source: ECONOMIC RESEARCH, ST. LOUIS FEDERAL RESERVE BANK).

4.4. Stochastic cost estimation model

The S-CEM is developed in @Risk (@Risk uses a MS Excel© interface). The uncertain parameters are interest rates, electricity prices; membrane costs; are specified as probability distributions (using @Risk functions) to represent the nature of their uncertainty. The empirical equations (26) to (35) described in model development section are used to determine the capital costs and operating costs from the design configuration details and operation parameters. Monte Carlo Method (MCM) is used to generate required number of *pseudo*-random numbers from the input probability distributions. The simulations are performed to determine the distribution of the total costs. Figure 5 gives a brief overview of the S-CEM.

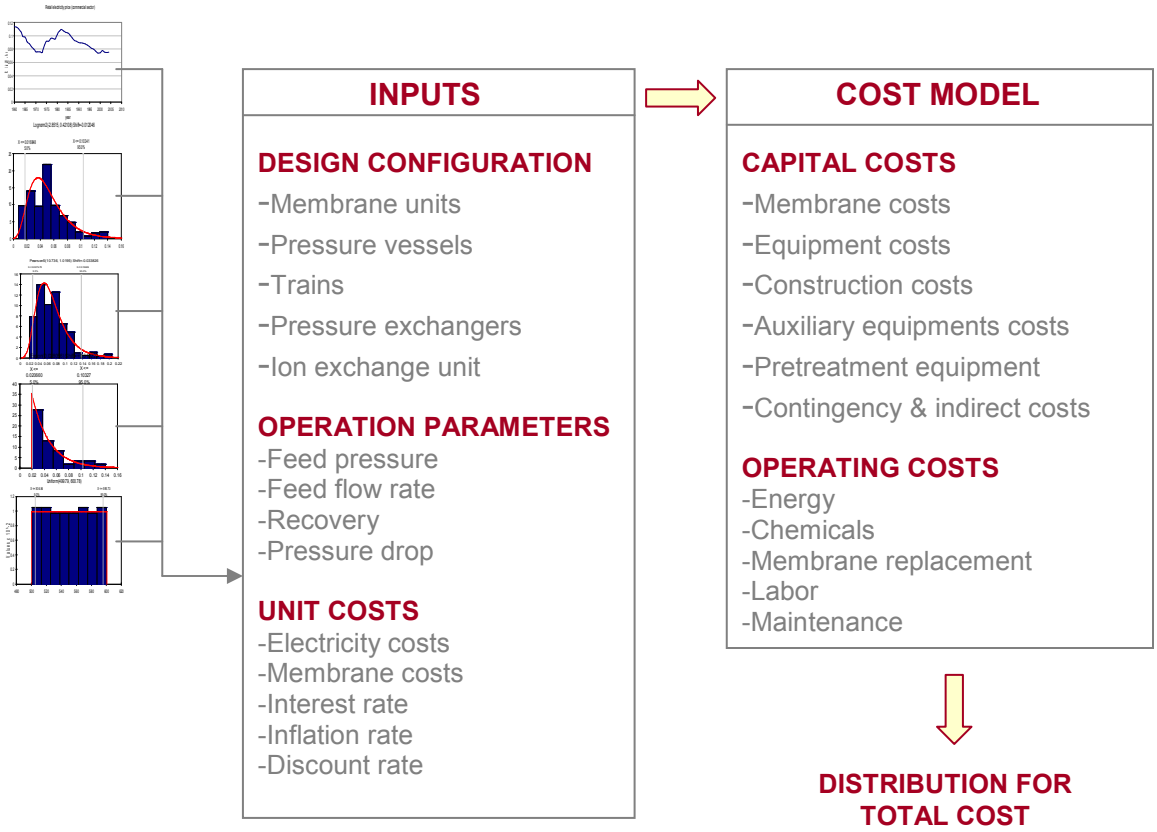

Figure 5. Schematic of stochastic cost estimation model developed in MS Excel ©. The simulations are performed using @Risk (simulation software embedded in MS Excel).

The random numbers generated from each distribution along with the design and operation parameter values are used to determine the capital costs and operating costs. The addition gives the total cost of water produced in terms of $\$/m^3$.

5. RESULTS AND DISCUSSION

5.1. Pilot-Scale Experimental Results

The pilot-scale experimental results are shown in Figure 6(a) and 6(b). The boron rejections varied from 82.9 to 98.3 % for RE4040-SH and from 84.6 to 98.9 % for RE4040-SR producing permeate water with boron concentration of 0.08 – 0.9 mg/L and 0.05 – 0.8 mg/L, respectively. The boron rejection was lowest at lowest pH (pH = 6.2) and at lowest pressure (600 Psi) and increased as both pH and pressure increased. The rejection was low for RE4040-SH as the hydraulic transport parameter (*A*) of this membrane was low as compared to RE4040-SR, leading to low recovery and high boron concentration in permeate water. As the feed pH is increased, the boron present as boric acid (H_3BO_3) in water is converted to borate ion ($H_2BO_3^-$) leading to higher rejection at higher pH. As feed pressure is increased, the recovery increases producing more permeate and with relatively less boron concentration. Therefore as pressure increases, the overall boron rejection increases.

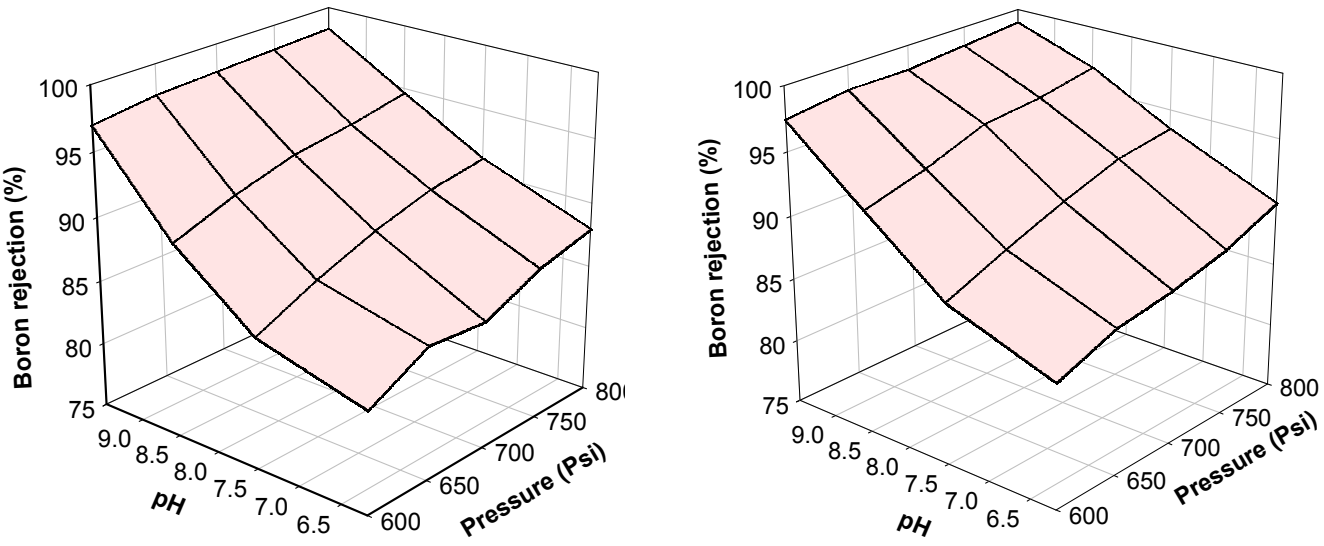

Figure 6. Boron rejection by a 4 inch (dia.) (a) RE4040-SH and (b) RE4040-SR pilot-scale RO membrane from (Saehan Inc.). Experiment was performed at operating conditions of feed pH ranging from 6.2 to 9.5, and feed pressure ranging from 600 to 800 psi. The overall permeate recovery was maintained constant at ~ 8 % (i.e. $Q_{pT}/ Q_{f0} = 0.08$) and temperature T at 25^{o}C.

5.2. Parameters

Hydraulic Transport Parameter (A) and the Solute (TDS) Transport Parameter (B)

The hydraulic permeability (A) and the solute (TDS) permeability (B) for RE4040-SR membrane module were determined by using the iterative algorithm developed in this study. The values for feed flow rate, feed (TDS) concentration and feed pressure were 50.3 m3/day, 33,000 mg/L and 800 psi respectively (obtained from

standard testing data provided by manufacturer, Saehan Inc.). These values with assumed values for A and B, i.e. 2.58×10^{-4} (m/(KPa·day)) and 1×10^{-3} (m/day) respectively, were used as inputs to the parameter estimation model. The standard testing data for pilot-scale spiral wound module available from manufacturers were used. The values obtained from the parameter estimation algorithm are 2.37×10^{-4} (m/(KPa·day)) and 1.5×10^{-3} (m/day) for A and B respectively.

Boron Transport Parameter (B_S)

The empirical constants $B_{s(H3BO3)25}$ and $B_{s(H2BO3-)25}$ to predict boron permeability ($B_{s(b)}$) were determined experimentally by Hyung and Kim (2006) for SRN flat membrane coupon (Hyung and Kim 2006). The values of $B_{s(H3BO3)25}$ and $B_{s(H2BO3-)25}$ are 0.0735 and 0.0076 [m/day; LT^{-1}], respectively. Due to high rejection of salts (TDS) by RO membranes a reflection coefficient σ was assumed to be equal to 1. However the reflection coefficient for boric acid (H_3BO_3) was 0.9949 [dimensionless] and for borate ion ($H_2BO_3^-$) was 0.9985 [dimensionless], for SRN membrane at temperature equal to 25°C. Since, these parameters are membrane specific and do not change with configuration or operating conditions, same were used for model simulations of pilot-scale and full scale process.

Friction parameters

A maximum pressure drop observed in pilot-scale experiments using a single

spiral wound module was 10 psi. This value was obtained from manufacturers (Saehan Inc.) specifications. Further using, a trial and error algorithm with a permissible error of ≤ 0.001 as convergence criteria, the brine and permeate friction parameters for SRN membrane were identified to be 5.183×10^{10} [$(1/m^2)$; L^{-2}] and 1.1×10^{9} [$(1/m^2)$; L^{-2}] respectively.

Mass Transfer Coefficient (k)

Four different mass transfer correlations suggested by Winograd *et.al.*, 1973; , Schock & Miquel, 1987; Mariñas and Urama, 1996; and Taniguchi and Kimura, 2000; respectively, were considered for the sensitivity analysis (Winograd, Solan *et al.,* 1973; Schock and Miquel, 1987; Marinas and Urama, 1996; Taniguchi and Kimura, 2000). The deviation in prediction of boron rejection was relatively minor and varied from 91.67 % (for Schock & Miquel) to 92.30 % (Mariñas) (Figure 7). Since, the mass transfer model developed by Winograd (1973) is the most basic model that was developed for mass transfer in narrow channels and accounts for presence of spacers, and the prediction results have no significant deviation in terms of boron rejection and recovery, this model was selected. The effect of different mass transfer correlations on the recovery are presented in Figure 8. The overall product recovery varied from 7.30 % to 10.05 % percent with no significant deviation.

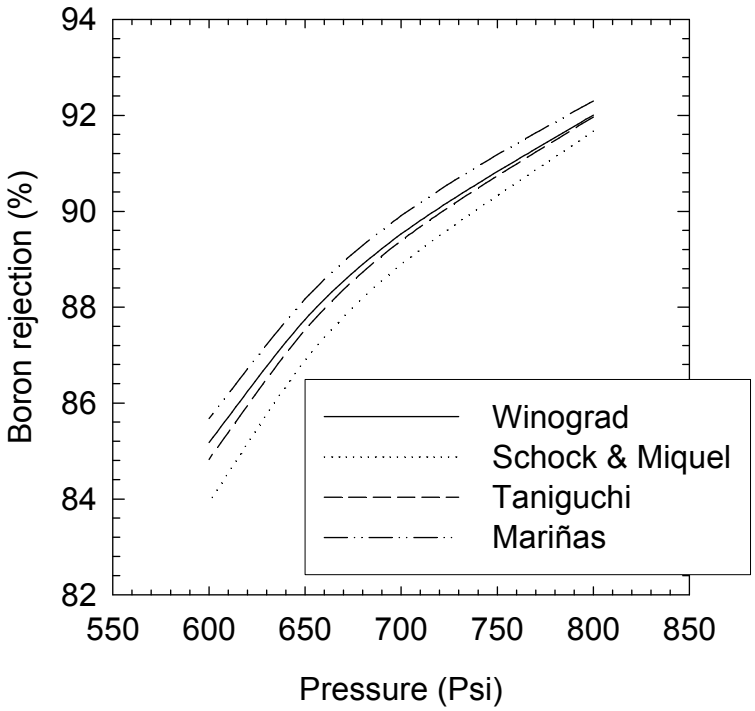

Figure 7. Boron rejection prediction by employing different mass transfer correlations at pH = 6.2 and temperature $T = 25^{o}$C.

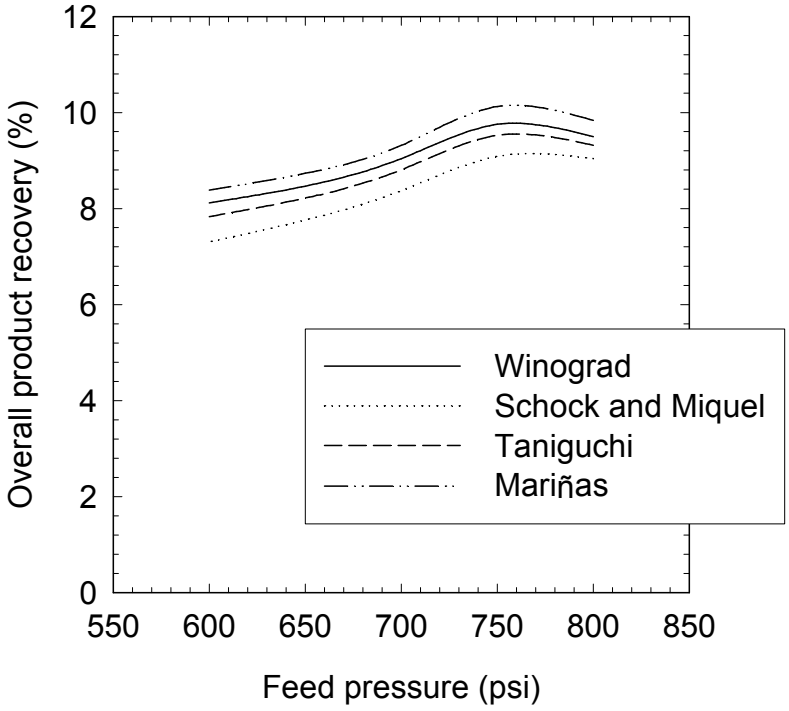

Figure 8. Overall product recovery prediction by employing different mass transfer correlations at pH = 6.2 and temperature $T = 25^{o}C$.

5.3. Model simulations and comparisons

Above parameters and the membrane characteristics listed in Appendix A and C respectively, were used as constants in the model for simulating the performance of a pilot-scale RE4040-SR membrane to reject boron in seawater. The operating conditions used for pilot-scale experiments, were used as the inputs to the simulation model. The input parameters are feed flow rate Q_{f0} [m^3/day; L^3T^{-1}], feed pressure P_{f0} [kPa; $ML^{-1}T^{-2}$],

feed salt (TDS) concentration C_{f0} [g/L; ML^{-3}], feed boron concentration C_{fB0} [g/L; ML^{-3}], feed pH [dimensionless], and feed temperature T [^{o}C; θ]. The feed flow rate was adjusted at a determined pressure for every experiment run, so as to get a target recovery of 8% (i.e. $Q_{pT}/ Q_{f0} = 0.08$), as the target recovery is the target parameter in full-scale processes. The boron concentration and salt (TDS) in feed water was maintained at 5 mg/L and 32.85 ± 0.17 g/L respectively, for the pilot-scale experiments. Same values were used as input for model simulations.

The results for model simulation and their comparison with observations are as shown in Figure 9(a) to 9(d). As seen from plots of boron rejection vs. pressure at different pH, the model simulation results were in excellent agreement with the experimental results. The boron rejection was low at pH = 6.2 and increased with the pH (pH = 9.5). The lowest rejection was observed at pH = 6.2 and pressure = 600 Psi as expected, and is equal to 87.71 %. And the highest boron rejection was observed at pH = 9.5 and pressure = 800 Psi, and is equal to 98.19 %. The product recovery varied from 8.14 % to 9.13 %, (as compared to 8 % for pilot-scale experiments) with an error of 1.8 - 14.2 %, which may be considered to be a good in terms of prediction by model simulations. The salt rejection (TDS) remained above 99 % as in case of pilot-scale experiments. The results for pilot-scale experiments are presented in Appendix B-I and B-II.

The maximum discrepancy between model prediction and pilot-scale experimental data was observed at pH = 6.2. At this pH, almost all of the boron is present as boric acid, which is a perfectly symmetrical non-polar molecule. Therefore it is predicted that, due to presence of imperfections and variability in structure of

membrane, there might be significant passage of boric acid molecules leading to low rejection, which is not accounted by the model, leading to a relatively high discrepancy. However, as pH increases, more borate ions are present which are rejected primarily by charge repulsion effect, and is predicted fairly by the model.

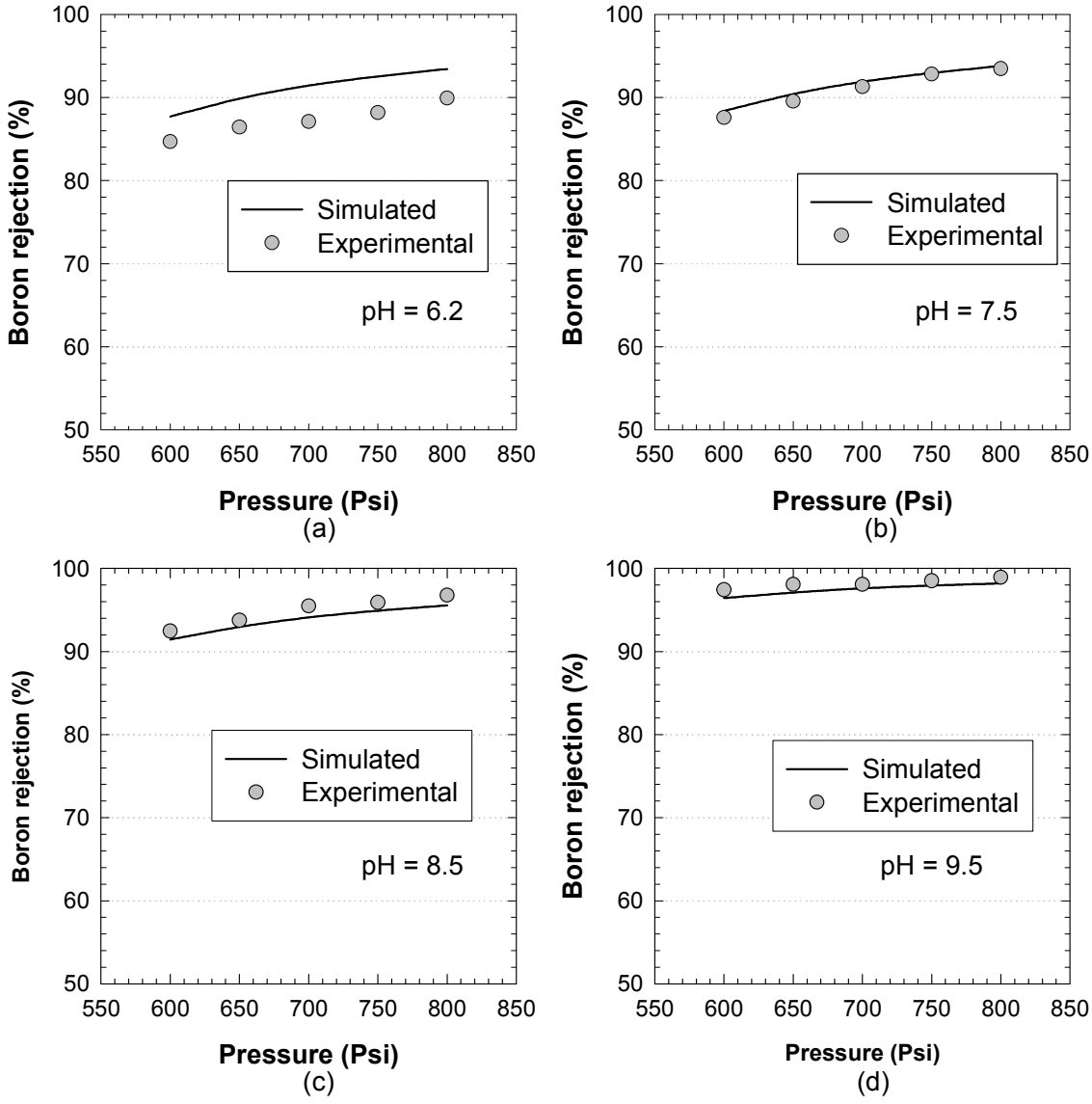

Figure 9. Comparison of boron rejection measured in pilot scale experiments and predicted by simulation model for pilot scale spiral wound RO membrane. (a) pH = 6.2 (b) pH = 7.5 (c) pH = 8.5 (d) pH = 9.5. For each experiment pressure was varied from 600 to 800 psi (600, 650, 700, 750, and 800 psi), with overall permeate recovery maintained constant at 8 % (i.e. $Q_{pT}/ Q_{f0} = 0.08$) and temperature T at 25^{o}C.

5.4. Cost simulations

5.4.1. Input probability distributions

The input probability distributions developed for the input parameters (for which data were available) are summarized in Table 1. Since no previous data were available, uniform distributions were assumed for membrane element costs, pressure vessel, high pressure pumps, ion-exchanger, pressure exchanger, trains cost, and pretreatment equipment costs. The minimum and maximum values for the uniform distribution were assumed to be -10% and +10% of the actual present cost respectively.

Table 3. Summary of the input probability models developed for interest rate, inflation rate, discount rate and electricity price.

Input parameter	Distribution	Chi-square value	p-value
Interest rate	Weibull	5.00	0.76
Inflation rate	Exponential	14.17	0.03
Discount rate	Lognormal2	5.93	0.66
Electricity price	Beta General	3.74	0.81

5.4.2. S-CEM simulation results

The cumulative distribution of the total cost, as net present value (NPV), is presented in Figure 10. As seen from the result the total cost of water produced (as NPV in $\$/m^3$) from each design option varies from approximately 5 $\$/m^3$ to 25 $\$/m^3$, and has

different probability of it being below a certain value. For example, the system IV, which is a double stage process, has the highest probability that its cost would remain below 10 $/m^3 as compared to other design options. System II (double pass process) has the highest cost and the lowest probability that its cost will remain below 10 $/m^3. Also, system design I has cost very close to system IV and has approximately equal or more risk.

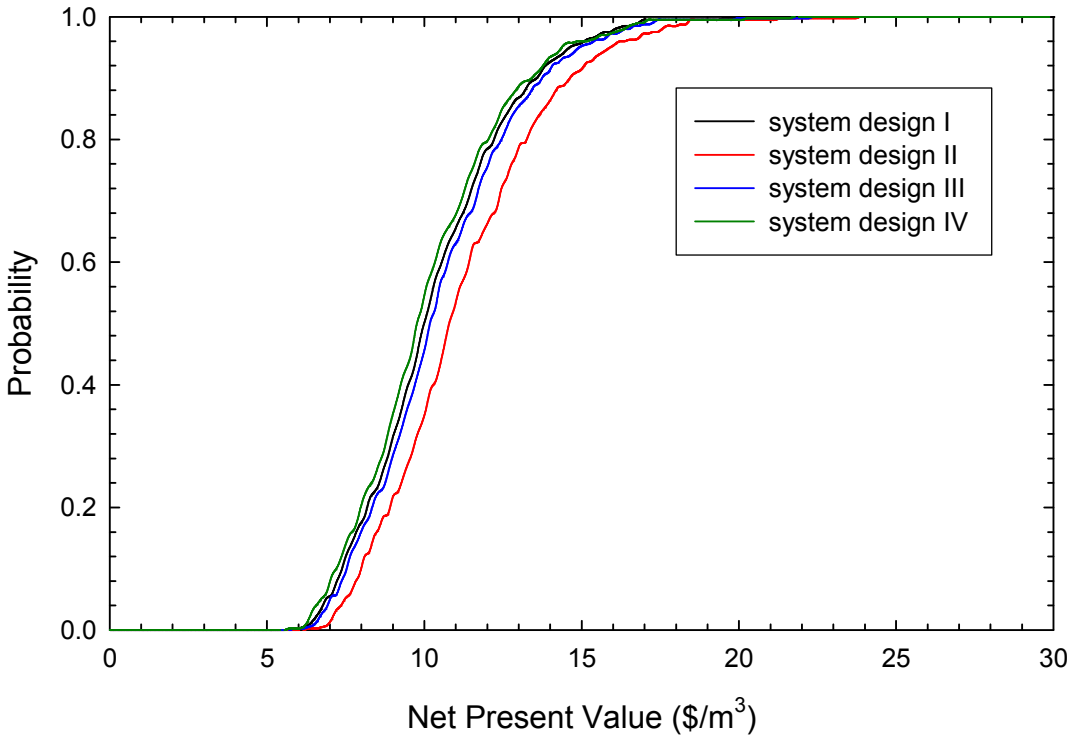

Figure 10. Cumulative distribution of the total cost (as NPV, in $/m^3) for system design options I to IV. Y-axis represents the probability and X-axis represents the total cost as net present value (NPV).

The summary of stochastic cost simulations is presented in Table 2. System IV has the lowest expected cost (mean) equal 10.26 $/m^3 and system IV has the highest expected cost equal to 11.32 $/m^3. Since, system IV has low capital costs (primarily due

to high recovery, and effectively less intake and pump costs) it presents the best option under given uncertainty as compared to other design options. The risk involved in terms of standard deviation, system I has the lowest risk (in terms of standard deviation), but the difference between the standard deviation for system IV is insignificant. Therefore system IV may be the best design option under given scenario of uncertainty in different input parameters. Please note that the purpose of this cost analysis study was to present an approach and not determine the actual cost of water. So the values presented here may vary significantly from the actual cost and the estimate may be considered as a study estimate (Class IV).

Table 4. Summary of S-CEM simulations for system designs I, II, III and IV.

Name	NPV / I	NPV / II	NPV / III	NPV / IV
Minimum	5.89	6.35	5.99	5.70
Mean	10.46	11.32	10.65	10.26
Maximum	21.98	23.86	22.42	21.81
Std Dev	2.41	2.62	2.46	2.43
Variance	5.80	6.86	6.03	5.92

To study the impact of various stochastic inputs on the total cost, regression sensitivity analysis is performed using @Risk. Figure 11 shows the relationship between the different inputs and total cost. As, seen from the figure, discount rate has the highest negative correlation with the total cost, with the total cost, and inflation rate has the highest positive correlation. Whereas the membrane cost has the least impact on the total cost.

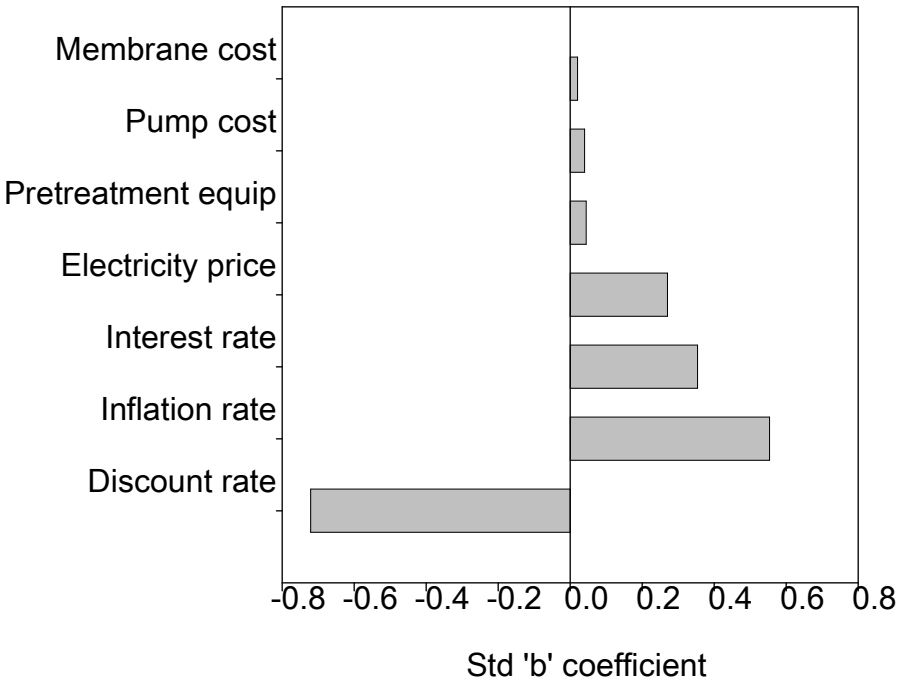

Figure 11. Regression sensitivity analysis to observe the effect different stochastic input parameters on total cost.

Discount rate, inflation rate, interest rate and electricity prices have been identified as the inputs that have significant effect on the total cost of water produced. The uncertainty in these inputs may change significantly and be large than presented by the input model developed based on previous data. Therefore, to further study the impacts of the change in uncertainties in the important input parameters i.e. discount rate, inflation rate, interest rate, and electricity price, a sensitivity analysis is performed.

5.4.3. Sensitivity Analysis

To quantify the effect of change in uncertainty, sensitivity analysis was performed to exemplify the variation observed in total cost (NPV, $\$/m^3$), by variation in uncertainty and expected value of inputs. Figure 12(a) and 12(b) show the effect of change in uncertainty and expected value of electricity price respectively. As seen from Figure 13(a), varying uncertainty having same expected value for electricity price has not effect of change in ranking of the systems (according to their expected total cost). This is because; the maximum value of electricity price was fixed at 11.4 cents/KW-hr. Later as seen from Figure 12(b), the maximum bound of the distribution was increased from 11.4 till 30 cents/KW-hr, leading to a corresponding increase in uncertainty and expected value of electricity price. This changes the order of ranking of systems and system I has the lowest expected cost and there is a significant increase in expected total cost for system IV (originally lowest expected cost) as compared to other systems. Therefore, an increase in uncertainty and expected total cost of the electricity price may have a significant effect on the ranking of systems. The increase in uncertainty (as variance) in discount rate has a similar effect on expected total cost of all the systems (Figure 12(c)). As the uncertainty (variance) increases (but the mean remains constant), there is an increase in expected total cost of all the systems. No change of order is observed in this case. In case of inflation rate, the input probability distribution that was developed was an exponential distribution and the mean and variance for this distribution change simultaneously with change in parameter β i.e. only variance cannot be changed keeping mean constant. Therefore, as shown in figure 12(d), as β increases, the expected total cost increases and at an value equal to 0.12 there is a change in order i.e. system I has the lowest expected total cost. (For an exponential distribution mean = β and variance = β^2).

Therefore, an insight is obtained on the effect of various parameters on the expected total cost

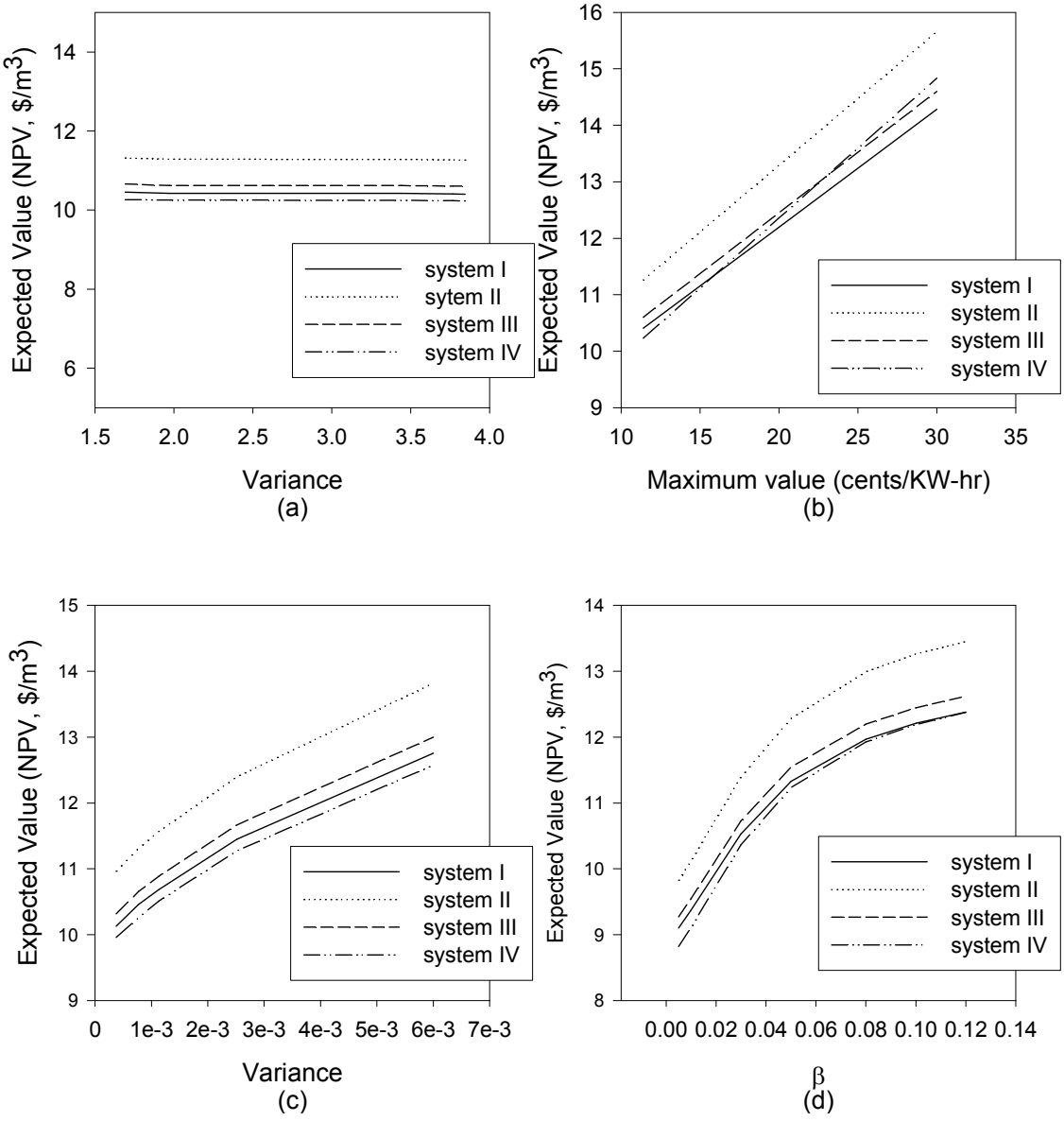

Figure 12. Sensitivity analysis to observe the effect of change in uncertainty of input parameters on total cost of water produced. (a) effect of change in uncertainty of electricity price, (b) effect of change in uncertainty and expected value of electricity price, (c) Effect of change in uncertainty of discount rate, and (d) effect of change in expected cost and uncertainty of inflation rate.

6. MODEL APPLICATIONS

6.1. Single spiral wound module

The model was further used to predict the performance of a single spiral wound module RE4040-SR (Saehan, Inc.) with respect to boron rejection, under varying operating conditions. First, pressure was varied from 600 to 1200 Psi in steps of 10 Psi and pH was varied from 6 to 12 in steps of 0.1. Other conditions were fixed at temperature, T = 25^{o}C; feed TDS concentration, C_{f0} = 33,000 mg/L; feed boron concentration, C_{fB0} = 5 mg/L; and feed flow rate = 200 m^3/day. As shown in Figure 14(a), the overall boron rejection varied from 81.72% at (pH = 6 and pressure = 600 Psi) to 99.4% (at pH = 12 and pressure 1200 Psi). As pressure is increased, water flux increases, leading to effective dilution of boron in permeate water and consequently increase in boron rejection. Also, as pH is increased, boron rejection increases rapidly. This is because as pH increases, the speciation changes and above pH = 8.68, most of the species present in water are borate ions. A contour plot as shown in Figure 13 (b) can be obtained from the 3D plot. The contour plot, showing iso-rejection lines, represents combinations of different pressure and pH to attain the same boron rejection with other conditions fixed. Similarly, the effect of the varying feed pressure and feed temperature are at fixed pH of 8.0 was simulated. Pressure showed a similar effect *i.e.* boron rejection increased with increasing pressure. The effect of increasing temperature was subsequent reduction in boron rejection. This may be explained as the temperature increases, the

diffusivity of boron increases and also there may be loosening of membrane, leading to high solute and solvent flux through the membrane.

The contour plot developed for specific base conditions can be used for prediction of boron rejection. *E.g.* given the operating conditions of pressure and pH, the range of boron rejection can be estimated, which would be helpful in quick predictions.

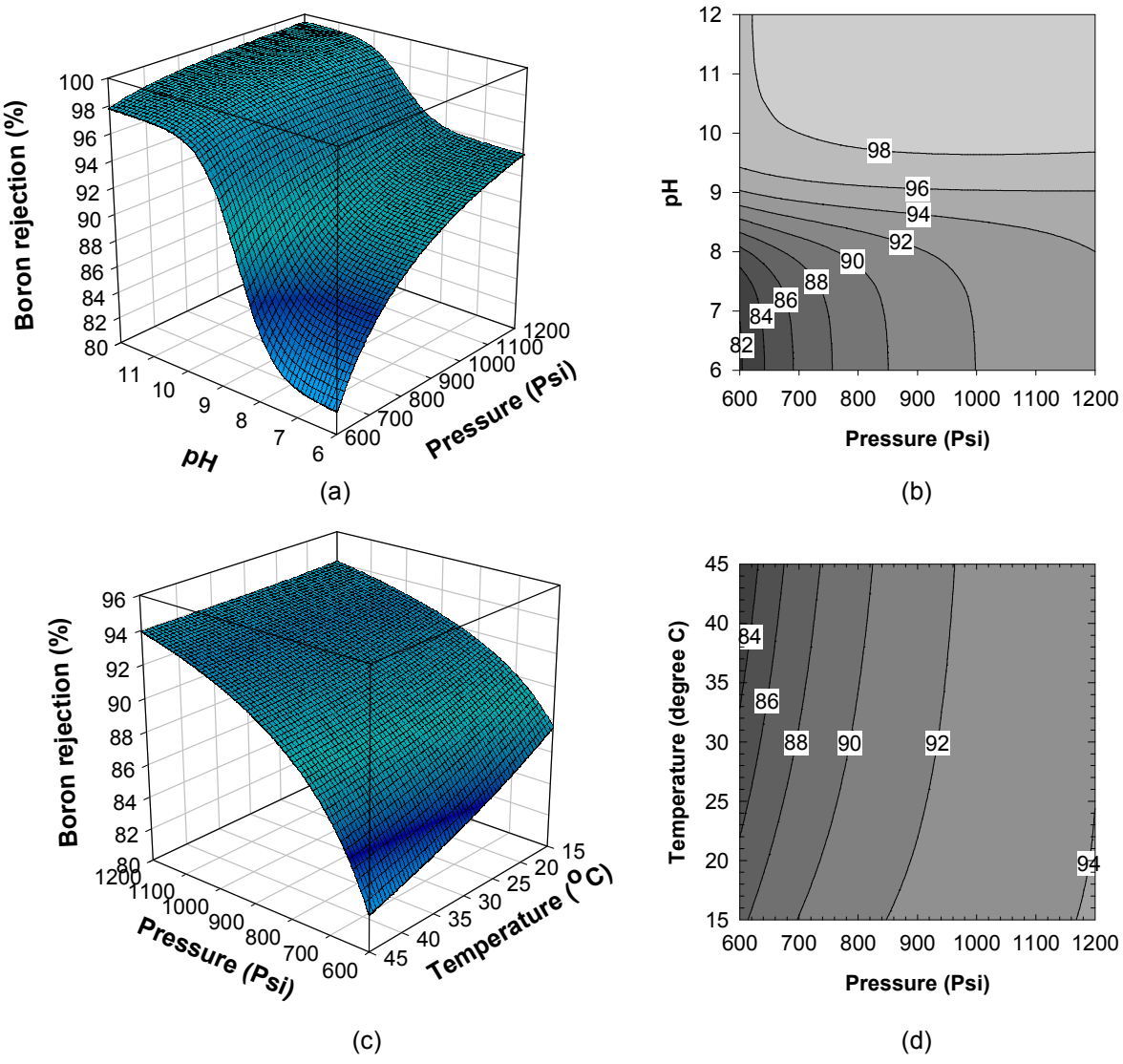

Figure 13. Simulation results for boron rejection by RE4040-SR pilot-scale SWRO membrane under varying operating conditions of feed pH and feed pressure (psi). The base conditions for the simulation were feed flow rate Q_{f0} = 200 m^3/day; feed salt (TDS)

concentration C_{f0} = 33,000 mg/L; feed boron concentration C_{fb0} = 5 mg/L; and temperature $T = 25^{o}C$.

6.2. Full-scale design option simulations

Four representative design options which are currently in practice were selected for full-scale simulation. The primary purpose of full-scale simulation was to determine the operating parameters study and further comparison by stochastic cost analysis. Figure 14(a) to 14 (d) shows the detailed design configuration for these design options.

(a) Feed water characteristics

The performance of four different design options by process simulation needs to be studied for same feed water characteristics that are representative of actual seawater conditions. The feed water characteristics are used as inputs to the deterministic process model along with the operating conditions and design configuration details. The important characteristics of the feed water required for the process simulation are listed in Table 3.

Table 5. Characteristics of feed water

(1)	Type	Seawater
(2)	Feed salt (TDS) concentration, (mg/L)	33,000
(3)	Feed boron concentration, (mg/L)	5
(4)	Feed pH	8.0
(5)	Feed temperature (^{o}C)	25

(a) Single-stage single pass

Figure 14(a) shows the schematic of a conventional single-pass RO process. It consists of a single pressure vessel holding 6-8 membrane elements in series targeting a recovery of 40-50 % in seawater desalination process. These systems are usually considered as low-medium recovery systems capable of producing permeate water with salt (TDS) concentrations below 500 mg/L. However, it is challenging for these systems to produce permeate water below 0.5 mg/L.

A single train consisting of a pressure vessel, holding 8 SWRO (RE8040-SR, Saehan Inc.) membrane elements in series, was considered for this simulation study. The parameters and the membrane characteristics for the RE8040-SR membrane element are provided in Table presented in the Appendix A. The design details and the operating parameters used for this system are provided in Table 4.

Table 4.System details and and operating conditions for single stage process design

(1)	Array configuration	Single-stage, Single-pass
(2)	Pressure vessel	8 SWRO elements in series
(3)	Spiral wound element	RE8040-SR (Saehan Inc.)
(4)	Feed pressure, Stage I, (psi)	800
(5)	Feed pressure, Stage II, (psi)	-
(6)	Feed flow rate, (m^3/day)	200

(b) Double-pass process

A schematic of a double-pass RO system is shown in Figure 14 (b) and details are provided in Table 5. The double-pass process typically consists of a leading SWRO unit (RO1) operating at a recovery of 40 to 50 % followed by a brackish RO unit (RO2)

operating at a recovery of 85 to 90 %. Since the feed to the RO2 process is the RO1 permeate (i.e., RO2 feed has low salinity), the RO2 unit operates at a relatively high flux (typically 20 GFD). The recovery of a double-pass process approaches the recovery of single-stage (single-pass) process as the recovery of the BWRO stage increases. As the water fed to the BWRO stage has salinity less than 500 mg/L, the number of elements required in the RO2 unit would be relatively small, thereby lowering marginal capital costs. In addition, depending on the temperature of and boron concentration in the feed water, it is possible that only a portion of RO1 permeate would be treated by the RO2 to produce a combined permeate that meets the provisional boron standard. Increasing the pH of RO2 feed beyond 9.5 (and up to 10) by adding sodium hydroxide as shown in the Figure 14(b) is commonly practiced to achieve 80-95 % boron rejection by the brackish membranes. Consequently, a double-pass system generally achieves a much higher level of boron reduction when compared with a single-pass system. For the cost analysis performed as part of this study, a system treating 16 % of RO1 permeate was considered.

Table 5. System details and and operating conditions for double pass process design

(1)	Array configuration	Double-pass
(2)	Pass I	SWRO (single stage)
(3)	Pass II	BWRO (7:3 array)
(2)	Pressure vessel, Stage I	8 SWRO elements in series
(3)	Spiral wound element	RE8040-SR (Saehan Inc.)
(4)	Feed pressure, Stage I, (psi)	800
(5)	Feed pressure, Stage II, (psi)	154
(6)	Feed flow rate, (m^3/day)	200

Hybrid (Ion-exchange) process

In this process, conventional single stage process is coupled with a boron-specific ion-exchanger. The permeate water from the RO stage is partially treated with a boron selective IX process, which typically produces water with boron concentration below 0.1 mg/L, which is far below the required water quality criteria (Redondo, Busch *et al.*, 2003). Increasing the pH of feed water, with an objective of achieving high boron rejection may lead to scaling of calcium and magnesium (Nadav, 1999). The advantage of this process is that the pH of the feed water does not adjustment. The product recovery is generally very high for Ion-exchange systems. In this study, 16 percent of permeate is treated with IX process. A typical hybrid IX process is shown in Figure 14(c). Details for the design option are provided in Table 6.

Table 6.System details and and operating conditions for Hybrid IX process design

(1)	Array configuration	Hybrid IX process
(2)	Pass I	SWRO (single stage)
(3)	Pass II	Boron selective IX process
(2)	Pressure vessel, Stage I	8 SWRO elements in series
(3)	Spiral wound element	RE8040-SR (Saehan Inc.)
(4)	Feed pressure, Stage I, (psi)	800
(5)	Feed pressure, Stage II, (psi)	14.5
(6)	Feed flow rate, (m^3/day)	200

Double- stage process

In a double stage process, the brine from the first stage is treated by SWRO membranes again in a second stage. The operating pressure for second stage is generally high as the brine from first stage has a very high concentration. The double stage systems generally are employed to perform at very high recovery of approximately 60-70%. Since the recovery is high, the capital costs of the systems are low as compared to other systems. However, the operating costs are high due to higher operating pressures. The details for the system are summarized in Table 7.

Table 7.System details and and operating conditions for double stage process design

(1)	Array configuration	Double-stage
(2)	Pass I	SWRO
(3)	Pass II	SWRO
(4)	Pressure vessel, Stage I	8 SWRO elements in series
(5)	Pressure vessel, Stage II	8 SWRO elements in series
(6)	Spiral wound element	RE8040-SR (Saehan Inc.)
(7)	Feed pressure, Stage I, (psi)	800
(8)	Feed pressure, Stage II, (psi)	1200
(9)	Feed flow rate, (m^3/day)	200

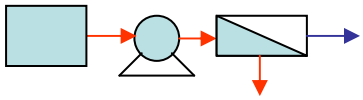

(a)

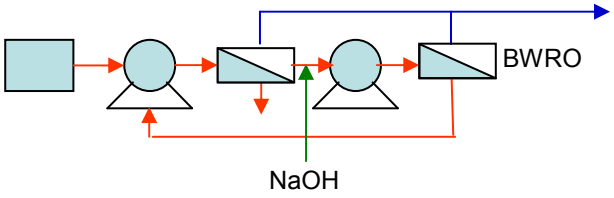

(b)

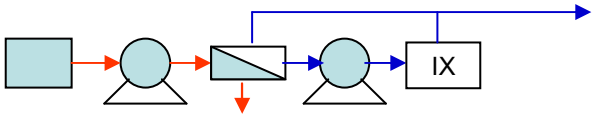

(c)

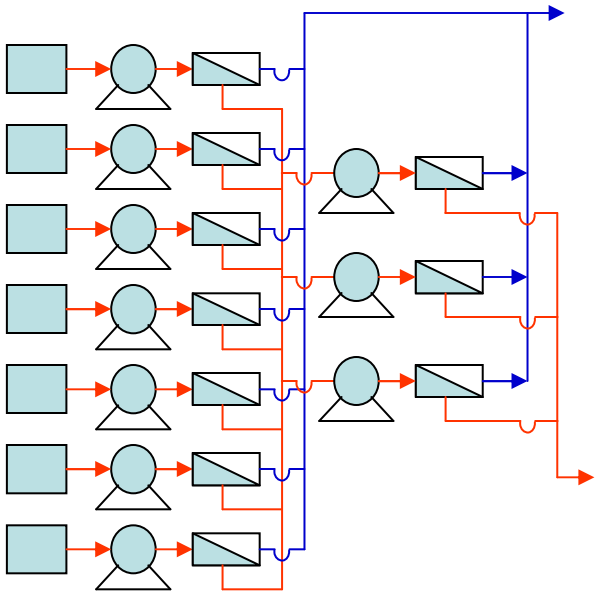

(d)

Figure 14. Representative design option used in seawater desalination by reverse osmosis. (a) Single pass-single stage (low recovery) (b) Double pass (c) Hybrid (single stage coupled with a boron specific ion-exchanger), and (d) Double stage (high recovery).

Simulation results

The predictions by the full-scale process model are listed in Table 8.

Table 8. Summary of results for simulation of four full-scale process design options, under standard operating conditions.

Option	Design option	Overall Permeate Recovery (%)	Overall Boron Rejection (%)	Overall TDS Rejection (%)	Feed pressure (psi) (Stage I/Pass I)	Feed Pressure (psi) (Stage II/PassII)
a/I	Single pass	46.44	87.13	99.58	800	-
b/II	Double pass	45.94	88.85	99.54	800	154
c/III	Hybrid	46.44	89.18	99.58	800	14.5
d/IV	Double stage	67.32	84.83	99.49	800	1200

As seen from the results (Table 8) every design option has boron rejection above 80 % producing permeate with boron concentration less than 1 mg/L. The double pass (system II) has the highest boron rejection with a rejection equal to 89.18 %. The double stage (system IV) has the lowest boron rejection at 84.83%. This is because, the feed water treated in second stage has a boron concentration almost twice (assuming 50% recovery in first stage) as compared to first stage, consecutively leading to more boron transport through membrane and high permeate boron concentration. However, at a rejection above 80% it will produce permeate water with boron concentration below 1 mg/L (feed boron concentration = 5 mg/L).

7. CONCLUSIONS

The ability of the mathematical model developed to predict the performance of a spiral wound SWRO membrane is verified with a set of pilot-scale experiments and is applications are theoretically explored. The deterministic model developed hereby can accurately predict the boron rejection performance of a spiral wound membrane module with given transport parameters. For the single spiral wound membrane SWRO simulations under different operating conditions following conclusions were drawn. Pressure and pH have a significant effect on the boron rejection performance of a pilot-scale SWRO membrane module. As pressure directly influences recovery of SWRO membrane module and pH influences the boron speciation (and consequently the rejection), the boron rejection for SWRO systems appears to be optimal at a higher recovery (pressure) and high pH, This model can be later modified to predict the performance of a full-scale process. However, the full-scale process may be a combination of two inherently different processes like a hybrid process (system design III) where membrane systems are integrated with other systems such as an IX process. In this case it would be helpful to have a process model to represent these different processes and could be coupled with SWRO process model to represent a complete process.

The double stage process included in this study (a high recovery system) is capable of producing water with boron concentration below 1 mg/L, with use of high boron rejection membranes. This is in confirmation with the earlier studies where the field sampling data for a double stage high recovery process, by Redondo *et al.* (2003) showed a high rejection above 90 percent, producing water with permeate boron

concentrations below 1 mg/L.

The cost analysis performed in this study was a novel approach to compare the costs of inherently different systems under uncertainty. Following conclusions were drawn from the cost analysis. A Single-stage (low recovery) process design and the double-stage (high recovery) process deign are the most cost-effective options and the risk associated with the total cost was least in case of single-stage process design which may prove the best system under current scenario. However, the capital costs for double stage process were significantly leas than other design options, as it was a high recovery process, which requires less feed flow and consequently less seawater intake and pretreatment costs. As the electricity price increases, single stage process proves to be the best one with lowest expected cost, as the cost of the double stage (high recovery) process increases rapidly. This is because the double stage (high recovery) process operates at high pressure and therefore requires more energy. The double pass and the hybrid process design appear to have relatively higher total costs as compared to other two systems. Therefore operating the single stage process (using high rejection membranes) at relatively high pressure to have a high recovery might be the most optimum solution for boron removal with a lowest expected cost and risk. The feed pH can be adjusted to obtain a specific rejection and therefore optimize the system.

REFERENCES

Bhattacharya, S. and S. T. Hwang (1997). "Concentration polarization, separation factor, and Peclet number in membrane processes." Journal of Membrane Science **132**(1): 73-90.

Cardona, E., S. Culotta, et al. (2003). "Energy saving with MSF-RO series desalination plants." Desalination **153**(1-3): 167-171.

Cardrew, L. (1998). "Membrane Processes: A Technology Guide."

CDHS (2006). "Drinking Water Notification Levels and Response Levels: An Overview." California Department Of Health Services (CDHS) - Drinking Water Program.

EPA (2005). "Drinking Water Contaminant Candidate List (CCL) 2." **2**.

Helal, A. M., A. M. El-Nashar, et al. (2003). "Optimal design of hybrid RO/MSF desalination plants - Part I: Modeling and algorithms." Desalination **154**(1): 43-66.

Hyung, Brown. J. C., Wilf M., Park J.S., Kim J.H. (2006). "A Report on Mechanstic Study on Boron " U.S. Bureau of Reclamation.

Hyung, H. and J. H. Kim (2006). "A mechanistic study on boron rejection by sea water reverse osmosis membranes." Journal of Membrane Science **286**(1-2): 269-278.

Hyung H., B. J. C., Park J.S., Wilf M., Kim J.H. (2006). "A mechanistic study on boron." US Department of Interior and Bureau of Reclamation.

Kim, S. and E. M. V. Hoek (2005). "Modeling concentration polarization in reverse osmosis processes." Desalination **186**(1-3): 111-128.

Lu, Y. Y., Y. D. Hu, et al. (2006). "Optimum design of reverse osmosis seawater desalination system considering membrane cleaning and replacing." Journal of Membrane Science **282**(1-2): 7-13.

Magara, Y., T. Aizawa, et al. (1996). "The behavior of inorganic constituents and disinfection by products in reverse osmosis water desalination process." Water Sci. Technol. **34**(9): 141-148.

Malek, A., M. N. A. Hawlader, et al. (1996). "Design and economics of RO seawater desalination." Desalination **105**(3): 245-261.

Marinas, B. J. and R. I. Urama (1996). "Modeling concentration polarization in reverse osmosis spiral-wound elements." Journal of Environmental Engineering-Asce **122**(4): 292-298.

Maskan, F., D. E. Wiley, et al. (2000). "Optimal design of reverse osmosis module networks." Aiche Journal **46**(5): 946-954.

Matsuura, T. (2001). "Progress in membrane science and technology for seawater desalination - a review." Desalination **134**(1-3): 47-54.

Nadav, N. (1999). "Boron removal from seawater reverse osmosis permeate utilizing selective ion exchange resin." Desalination **124**(1-3): 131-135.

Parekh, B. S. (1988). "Reverse Osmosis Technology - Application for High Purity Water Production."

Redondo, J., M. Busch, et al. (2003). "Boron removal from seawater using FILMTEC (TM) high rejection SWRO membranes." Desalination **156**(1-3): 229-238.
Sagiv, A. and R. Semiat (2004). "Analysis of parameters affecting boron permeation through reverse osmosis membranes." Journal of Membrane Science **243**(1-2): 79-87.
Schock, G. and A. Miquel (1987). "Mass-Transfer and Pressure Loss in Spiral Wound Modules." Desalination **64**: 339-352.
Senthilmurugan, S., A. Ahluwalia, et al. (2005). "Modeling of a spiral-wound module and estimation of model parameters using numerical techniques." Desalination **173**(3): 269-286.
Spiegler, K. S. and O. Kedem (1966). "Thermodynamics of hyperfiltration(reverse osmosis): criteria for efficient membranes." Desalination **1**: 311-326.
Strathmann, H. (1981). "Membrane Separation Processes." Journal of Membrane Science **9**(1-2): 121-189.
Strathmann, H. (2001). "Membrane separation processes: Current relevance and future opportunities." Aiche Journal **47**(5): 1077-1087.
Taniguchi, M., Y. Fusaoka, et al. (2004). "Boron removal in RO seawater desalination." Desalination **167**: 419-426.
Taniguchi, M. and S. Kimura (2000). "Estimation of transport parameters of RO membranes for seawater desalination." Aiche Journal **46**(10): 1967-1973.
Taniguchi, M., M. Kurihara, et al. (2001). "Boron reduction performance of reverse osmosis seawater desalination process." Journal of Membrane Science **183**(2): 259-267.
WHO (1998). Addendum to Guidelines for Drinking Water Quality Geneva.
Wilf, M. and C. Bartels (2005). "Optimization of seawater RO systems design." Desalination **173**(1): 1-12.
Wilf, M. and K. Klinko (2001). "Optimization of seawater RO systems design." Desalination **138**(1-3): 299-306.
Winograd, Y., A. Solan, et al. (1973). "Mass-Transfer in Narrow Channels in Presence of Turbulence Promoters." Desalination **13**(2): 171-186.

APPENDIX A

Membrane module characteristic and performance parameters obtained from membrane manufacturer.

	Pilot scale experiments	Full-scale simulation
Manufacturer	Saehan, Kyungsan, Korea	Saehan, Kyungsan, Korea
Model	RE4040-SR	RE8040-SR
Element configuration	Spiral wound	Spiral Wound
Membrane type	Thin Film Composite (TFC)	Thin Film Composite (TFC)
Material	Polyamide (PA)	Polyamide (PA)
Effective membrane area (m^2)	6.9	34.4
Feed channel height (m)	8.6×10^{-4}	8.6×10^{-4}
Permeate channel height (m)	4.0×10^{-4}	4.0×10^{-4}
Friction parameter for feed channel (k_{fb}), [$(1/m^2)$; L^{-2}]	5.183×10^{10}	5.183×10^{10}
Friction parameter for permeate channel (k_{fp}), [$(1/m^2)$; L^{-2}]	1.1×10^{9}	1.19
Applied pressure (MPa)	5.51	5.51
Solute / concentration (mg/L)	NaCl / 32000	NaCl / 32000
Temperature (ºC)	25	25
Ph	6.5 ~ 7.0	6.5 ~ 7.0
Operation time (min)	30	30
Permeate flow rate (m^3/day)	4.5	22.7
Salt rejection (%)	99.6	99.6
Permeate recovery (%)	8.0	8.0

APPENDIX B-I

Boron rejection and conductivity rejection experimental data for pilot-scale SH (RO membrane, Saehan Inc.) at varying feed pH and feed pressure. The overall permeate recovery was maintained constant at ~ 8 % (i.e. $Q_{pT}/ Q_{f0} \sim 0.08$) and temperature T at 25^{o}C

	Pressure (Psi)	Permeate Flow Rate (m^3/day)	Conductivity Rejection (%)	Boron Rejection (%)
pH 6.2	800	3.04	99.76	87.96
	750	2.59	99.74	86.87
	700	2.42	99.71	84.9
	650	2.16	99.67	85.34
	600	1.82	99.63	82.93
pH 7.5	800	3.05	99.76	91.07
	750	2.51	99.74	90.41
	700	2.40	99.72	89.11
	650	2.10	99.67	87.36
	600	1.75	99.61	85.19
pH 8.5	800	3.00	99.77	94.6
	750	2.66	99.75	93.74
	700	2.42	99.72	93.09
	650	2.08	99.68	91.79
	600	1.76	99.63	90.06
pH 9.5	800	3.09	99.76	98.27
	750	2.77	99.74	98.06
	700	2.43	99.71	97.84
	650	2.08	99.67	97.62
	600	1.82	99.63	96.98

APPENDIX B-II

Boron rejection and conductivity rejection experimental data for pilot-scale SRN (RO membrane, Saehan Inc.) at varying feed pH and feed pressure. The overall permeate recovery was maintained constant at ~ 8 % (i.e. $Q_{pT}/ Q_{f0} \sim 0.08$) and temperature T at 25^{o}C

	Pressure (Psi)	Permeate Flow Rate (m^3/day)	Conductivity Rejection (%)	Boron Rejection (%)
pH 6.2	800	4.02	99.73	89.93
	750	3.57	99.71	88.18
	700	3.34	99.68	87.09
	650	2.74	99.65	86.43
	600	2.30	99.60	84.68
pH 7.5	800	4.00	99.73	93.46
	750	3.57	99.71	92.81
	700	3.28	99.68	91.29
	650	2.70	99.64	89.54
	600	2.26	99.57	87.58
pH 8.5	800	4.04	99.74	96.76
	750	3.57	99.71	95.90
	700	3.15	99.69	95.46
	650	2.56	99.66	93.74
	600	2.27	99.60	92.44
pH 9.5	800	4.02	99.74	98.92
	750	3.58	99.71	98.49
	700	3.22	99.68	98.06
	650	2.56	99.65	98.06
	600	2.27	99.60	97.41

APPENDIX C

Parameters for model simulations

Parameter	Value
Hydraulic transport parameter (A), [$m^3/(m^2 \cdot Kpa \cdot day)$; $M^{-1}L^2T$]	2.37×10^{-4}
Solute transport parameter for salt (B), [m/day; LT^{-1}]	1.5×10^{-3}
Reflection coefficient for salt (σ), [dimensionless]	1
Temperature (T), ^oC	25
Solute transport parameter for boric acid (H_3BO_3) at 25^oC for SRN membrane ($B_{s(H3BO3)25}$), [m/day; LT^{-1}]	0.0735
Solute transport parameter for borate ($H_2BO_3^-$) estimated at 25^oC for SRN membrane ($B_{s(H2BO3-)25}$), [m/s; LT^{-1}]	0.0076
Reflection coefficient of boric acid (H_3BO_3) at 25^oC for SRN membrane ($\sigma_{(H3BO3)}$)	0.9949
Reflection coefficient of boric acid ($H_2BO_3^-$) at 25^oC for SRN membrane ($\sigma_{(H2BO3-)}$), [dimensionless]	0.9985

APPENDIX D

Parameter estimation algorithm used to determine A and B values from pilot-scale experimental data.